
# BRNO UNIVERSITY OF TECHNOLOGY
VYSOKÉ UČENÍ TECHNICKÉ V BRNĚ

## FACULTY OF MECHANICAL ENGINEERING
FAKULTA STROJNÍHO INŽENÝRSTVÍ

## INSTITUTE OF PHYSICAL ENGINEERING
ÚSTAV FYZIKÁLNÍHO INŽENÝRSTVÍ


# FABRICATION AND APPLICATION OF GRAPHENE-METAL HETEROSTRUCTURES IN BIOSENSING BY SURFACE ENHANCED RAMAN SPECTROSCOPY

VÝROBA A VYUŽITÍ GRAFEN-KOVOVÝCH HETEROSTRUKTUR V BIOSENZORICE POVRCHEM ZESÍLENÉ RAMANOVY SPEKTROSKOPIE

BACHELOR'S THESIS
BAKALÁŘSKÁ PRÁCE


AUTHOR
AUTOR PRÁCE
Veronika Hegrová

SUPERVISOR
VEDOUCÍ PRÁCE
Ing. Martin Konečný



BRNO 2017

VYSOKÉ UČENÍ TECHNICKÉ V BRNĚ
FAKULTA STROJNÍHO INŽENÝRSTVÍ

# Zadání bakalářské práce

| | |
|---|---|
| Ústav: | Ústav fyzikálního inženýrství |
| Studentka: | **Veronika Hegrová** |
| Studijní program: | Aplikované vědy v inženýrství |
| Studijní obor: | Fyzikální inženýrství a nanotechnologie |
| Vedoucí práce: | **Ing. Martin Konečný** |
| Akademický rok: | 2016/17 |

Ředitel ústavu Vám v souladu se zákonem č.111/1998 o vysokých školách a se Studijním a zkušebním řádem VUT v Brně určuje následující téma bakalářské práce:

## Výroba a využití grafen-kovových heterostruktur v biosensorice povrchem zesílené Ramanovy spektroskopie

**Stručná charakteristika problematiky úkolu:**

Grafen je dvoudimenzionální materiál sestávající se z uhlíkových atomů uspořádaných v hexagonální mřížce. Díky svým unikátním elektrickým a mechanickým vlastnostem se rychle stal jedním z nejrozšířeněji studovaných materiálů s celou řadou možných uplatnění od elektrotechniky až po biochemické a biomedicínské aplikace. V biochemických a biomedicínských aplikacích se například jedná o možnost využití grafenu v oblasti senzoriky pro detekci biomolekul, kde byly mimo jiné studovány zesilující účinky grafenu na Ramanův rozptyl molekul adsorbovaných na jeho povrchu. Jedná se o tzv. povrchem zesílenou Ramanovu spektroskopii (SERS – Surface Enhanced Raman Spectroscopy). Metoda SERS je spektroskopická metoda umožňující detekci molekul i při velmi nízkých koncentracích díky využití speciálně upravených povrchů zesilujících Ramanův rozptyl. Povrchy, popřípadě substráty, zesilující Ramanův rozptyl se nazývají SERS aktivní a jsou nejčastěji připravovány na podložním substrátu ve formě kovových nanostruktur (nanokuličky, nanodisky, nanotyčinky atd.). V posledních letech přitáhla velkou pozornost také možnost přípravy grafen-kovových heterostruktur kombinujících zesilující účinky jak klasických kovových nanostruktur, tak i samotného grafenu.

**Cíle bakalářské práce:**

1) Proveďte literární rešerši uvedené problematiky týkající se využití grafenu v oblasti metody SERS.
2) Vyrobte grafen-kovové heterostruktury s využitím zlatých koloidních nanočástic a CVD grafenu.
3) Výsledné grafen-kovové heterostruktury analyzujte pomocí Ramanovy spektroskopie. Dále naneste na připravené heterostruktury roztok Rhodaminu 6G a pokuste se jej detekovat pomocí metody SERS.
4) Zvažte možnost využití jiných 2D materiálů (např. MoS2, WSe2) při výrobě podobných heterostruktur vhodných pro metodu SERS.

**Seznam doporučené literatury:**

Ling X. et al., Can Graphene be used as Substrate for Raman Enhancement?, Nano Letters 10, 553-561 (2010), DOI: 10.1021/nl903414x

Xu W. et al., Graphene-Veiled Gold Substrate for Surface-Enhanced Raman Spectroscopy, Advance Materials 25(6), 928-933 (2013) DOI: 10.1002/adma.201204355

Ling X. et al., Lighting Up the Raman Signal of Molecules in the Vicinity of Graphene Related Materials, Accounts of Chemical Research 48, 1862-1870 (2015) DOI: 10.1021/ar500466u

Kang L. et al., Recent progress in the applications of graphene in surface-enhanced Raman scattering and plasmon-induced catalytic reactions, Journal of Materials Chemistry C 3, 9024-9037 (2015)

Kolibal M. et al., Guided Assembly of Gold Colloidal Nanoparticles on Silicon Substrates Prepatterned by Charged Particle Beams, ACS Nano 6 (11), 10098–10106 (2012), DOI: 10.1021/nn3038226

Termín odevzdání bakalářské práce je stanoven časovým plánem akademického roku 2016/17

V Brně, dne

L. S.

prof. RNDr. Tomáš Šikola, CSc.
ředitel ústavu

doc. Ing. Jaroslav Katolický, Ph.D.
děkan fakulty

**Abstract**
This thesis deals with fabrication of graphene/metal heterostructures and their application in biosensing by surface-enhanced Raman spectroscopy. The heterostructures are fabricated by selective deposition of gold colloidal nanoparticles onto silicon substrate, where the termination of both the gold colloidal solution and the silicon surface is controlled. Further, the assembled gold colloids are overlaid by graphene monolayer. The experiments have proved, that it is possible to observe the presence of biomolecules at very low concentrations if the parameters of graphene/metal heterostructures are well selected. The combination of both graphene and metal SERS properties have demonstrated their appropriateness for utilization in bisensing.

**Keywords**
SERS, graphene, graphene/metal heterostructure, AuNPs, rhodamine, biosensors

**Abstrakt**
Tato práce se zábývá výrobou grafen/kovových heterostruktur a jejich využitím v biosenzorice pomocí povrchem zesílené Ramanovy spektroskopie. Heterostruktury jsou vyráběny selektivní depozicí zlatých koloidních nanočástic na křemíkový substrát. Samotný proces depozice je založen na řízené terminaci zlatého koloidního roztoku i křemíkového povrchu. Nanesené zlaté kuličky jsou následně překryty vrstvou grafenu. Bylo experimentálně ověřeno, že s pomocí vhodně zvolených parametrů grafen/kovových heterostruktur je možné pozorovat přítomnost biomolekul o velmi nízkých koncentracích, a tedy heterostruktury využít k biodetekci.

**Klíčová slova**
SERS, grafen, grafen/kovové heterostruktury, AuNPs, rhodamin, biosenzorika

HEGROVÁ, V. *Fabrication and application of graphene-metal heterostructures in biosensing by Surface Enhanced Raman Spectroscopy.* Brno University of Technology, Faculty of Mechanical Engineering, 2017, p. 37. Supervisor Ing. Martin Konečný.

I declare that my bachelor's thesis "Fabrication and application of graphene-metal heterostructures in biosensing by surface enhanced Raman spectroscopy" has been composed solely by myself under supervisor of bachelor's thesis and that the thesis has not been submitted for any other degree or professional qualification. I confirm that the work submitted is my own, except where work of jointly–authored publications has been included. My contribution to this work and that of the other authors have been explicitly indicated below. I confirm that appropriate credit has been given within this thesis where reference has been made to the work of others.

Veronika Hegrová

I wish to express my sincere gratitude to Ing. Martin Konečný for providing me with all the necessary facilities, such as the guidance while performing the experiments and several corrections while writing this thesis. I am also grateful to Ing. Pavel Procházka for the fabrication and to Ing. Jakub Piastek for the assembly of graphene on my samples. Also, part of the work was performed with support of CEITEC Nano Research Infrastructure, Brno University of Technology. Lastly, I would like to thank my family and friends for the unceasing encouragement, support and attention.

Veronika Hegrová

# Contents

**Introduction** **3**

**1 SERS** **5**
1.1 Raman spectroscopy . . . . . 5
1.2 Introduction to SERS . . . . . 6
1.3 Application of SERS . . . . . 8

**2 Graphene in SERS** **11**
2.1 Graphene . . . . . 11
2.1.1 Structure and electrical properties of graphene . . . . . 11
2.1.2 Raman spectrum of graphene . . . . . 13
2.2 Utilization of graphene in SERS . . . . . 14

**3 Experimental part** **17**
3.1 Fabrication of graphene/metal heterostructures for SERS . . . . . 17
3.1.1 Deposition of gold colloids on Si-substrate with native oxide on the surface . . . . . 18
3.1.2 Deposition of AuNPs on $SiO_2$ . . . . . 23
3.1.3 Fabrication of graphene and its transfer on Au colloids . . . . . 23
3.2 Raman spectroscopy on graphene/AuNPs heterostructures . . . . . 25
3.3 SERS study of rhodamine on graphene/AuNPs heterostructures . . . . . 27

**Conclusion** **29**

**Bibliography** **31**

**List of abbreviations** **37**

# Introduction

Recently in nanotechnology, thin 2D materials became a subject of many discussions. In 2004 [1, 2], for a long time theoretically described monolayer of graphene was isolated from thick graphite. Thanks to the exceptional properties, graphene started to be experimentally studied in several branches. The structure and electrical properties of graphene make it a prospective material to partially replace silicon in electronic industry. Further, graphene has shown to be a suitable substrate in surface-enhanced Raman spectroscopy (SERS), where the weak inelastic Raman scattering is enhanced by plasmonic nanostructures. The utilization of graphene enables to uncover the SERS mechanisms and to improve the detection properties. Other favorable properties of graphene for SERS measurements are fluorescence quenching, biocompatibility and chemical stability [3, 4].

An interesting task and the aim of this thesis is to combine graphene and classical plasmonic nanostructures to fabricate a novel type of the substrate for sensing. The thesis is divided into three sections, where the first two theoretically summarize the fundamental features and application of the SERS technique and of graphene. Graphene in SERS is often used to lower the fluorescence of metal species, which overlaps the measured Raman spectrum. The experimental section focuses on fabrication and application of the graphene/metal heterostructures. The metallic compound used in heterostructures are gold colloidal nanoparticles of different sizes. To fabricate the heterostructures, it was necessary to adhere gold colloids on the substrate and cover them by graphene. The prepared graphene/metal heterostructures were further characterized and utilized for the SERS sensing of rhodamine. The goal was to find the lowest possible concentration of rhodamine detectable on the fabricated heterostructures. The experimental section summarizes all the results of graphene characterization and rhodamine examination.

# 1. Surface Enhanced Raman Spectroscopy

## 1.1. Raman spectroscopy

Raman Spectroscopy is an important non-destructive optical method used in plenty of branches such as chemistry [5], biochemistry [6,7], microbiology [8,9], medicine [10] or surface physics [11]. The main principles of this analytical method are based on the inelastic scattering of the light.

When a molecule is irradiated by an electromagnetic wave, the most of the radiation is scattered elastically with equal energy. This type of scattering is called Rayleigh scattering [12]. Nevertheless, a small fraction of photons is scattered inelastically. It is approximately one of $10^6 - 10^8$ impacted photons [13,14]. The first theories of inelastic (later called Raman) scattering were predicted by A. Smekal in 1923 [15]. In 1928, experimental verification was completed by C. V. Raman, who was awarded the Nobel Prize in 1930 for it [16–18].

The inelastically scattered photons cause the transition of a molecule to the excited or deexcited vibrational-rotational state. The energy change of the molecule within the vibrational levels perfectly matches with the energy difference of the impacted and the inelastically scattered photon [11]. When the scattered photon has lower energy than the impacted (= negative energy difference of the photons), the molecule goes to the excited state. This state belongs to the Stokes line, which is one of three peaks in the characteristic spectrum of scattered light (see the Figure 1.1). The Stokes line occurs on the sideband of Rayleigh line with much lower intensity ($(10^5 - 10^{12})$ times less [19]). On the other side of Rayleigh line is located the anti-Stokes line with even lower intensity than the Stokes line. The anti-Stokes line appears, when a molecule goes from the excited state to deexcited with positive energy difference of photons [13,14]. Raman spectroscopy is more often focused on the Stokes line thanks to the fact, that most of the molecules are in the ground state, which corresponds to higher intensity of the peak in the spectrum.

Raman Spectroscopy observes samples by characterizing vibrational and rotational states of molecules. Each particular molecule has unique fingerprints in the characteristic spectrum – Raman spectrum [20,21]. Raman spectrum typically represents the intensity of scattered light in dependence on Raman shift in reciprocal centimeters, which corresponds to the energy difference of the transition. The energy values are determined by the weight of the elements which create the molecule and by the force of mutual interaction. Therefore, the substances can be clearly distinguished and analyzed by detecting their fingerprints in Raman spectrum [22]. From the mutual intensity and the position of the peaks, it is possible to determine the properties of the material such as the composition and the spatial structure [13], type and carrier density [23], or tension and local mechanical stress of measured sample [24]. It is a common method used in Solid State Physics, but with benefits it can also be used for samples in different forms like liquids, gases and microscopic surfaces [25,26].

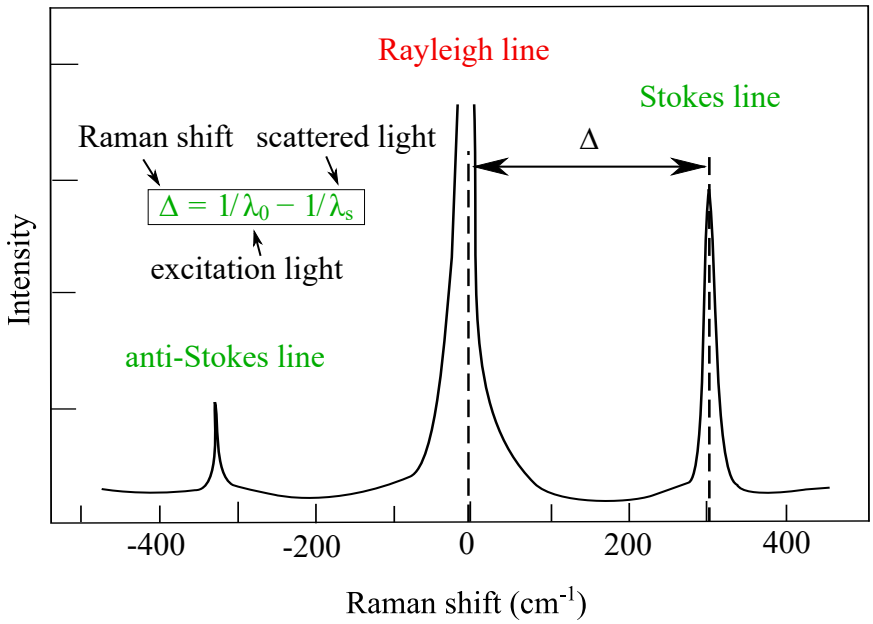


**Figure 1.1:** Scheme of Raman spectrum excited by laser $\lambda_0$ (nm). The graph shows dominant elastic Rayleigh scattering with inelastic Raman scattering on its sidebands. Taken and modified from [27].

## 1.2. Introduction to Surface-enhanced Raman spectroscopy

The advantage of previously discussed Raman spectroscopy is in easy and fast chemical analysis. This method is used for observation of chemical composition of substances and for chemical and bio-sensing [5–7]. On the other hand, the disadvantage is a very low intensity of the optical signal. Therefore, the aim is to enhance the Raman signal. One of the options is surface-enhanced Raman spectroscopy (SERS), which utilizes plasmonic nanostructures for the enhancement of the Raman signal.

The most common plasmonic nanostructures are metal nanoparticles with the size of hundreds of nanometers in the maximum [28]. These nanoparticles evince plasmonic resonance when irradiated by the light of specific wavelength [29, 30]. This resonance enhances the near electromagnetic field in the surroundings of the nanostructures (for example nanorods, spheres, nanoshells, etc. [31]) in order $10^3$ for one nanoparticle [32]. If the inspected substance is presented in the enhanced field, the Raman signal of this substance is enhanced as well.

The plasmonic resonance are collective oscillations of free electrons in the metal, so called surface plasmon polaritons (SPP) [33]. If they are space limited by nanostructure, the oscillations are localized only on the nanoparticle. The electron oscillations are then called localized surface plasmons (LSP) [34]. The plasmon resonance frequency of LSP depends in the simplest approximation on three parameters: on the material, the size and the shape of nanoparticles.

Every metal contains a different concentration of free electrons, therefore the plasmon resonance frequency LSP depends on the material of nanoparticles [35]. The materials with high concentration of free electrons have the resonance frequency shifted to higher frequencies (to shorter wavelengths). Because the majority of Raman spectroscopy works in the visible range of electromagnetic spectrum, the most suitable materials for nanoparticles in SERS are those with the highest concentration of free electrons – alluminium, silver and gold [36]. Furthermore, gold is a material, which does not oxide, but is easy to functionalize. On the surface of gold, it is facile to assemble distinct biomolecules, on whose the SERS is primary focused [37]. For these reasons, in the experimental part of this bachelor's thesis the gold colloidal nanoparticles will be utilized.

However, to fulfill the conditions of plasmonic resonance frequency in visible range, it is not enough only to select a type of the material. It is necessary to choose a specific size of nanoparticles with respect to the selected shape. The orientation of the free electron oscillations in the metal nanoparticles corresponds to the vector orientation of electric intensity of the light (polarization of light) [38]. Therefore, it is suitable to choose the shape of nanoparticles, which is independent on the polarization. This meets symmetrical nanoparticles such as spheres. The advantage of spherical nanoparticles is further their commercial availability in form of colloidal solution. Moreover, the price of the colloidal solution has recently been very low with good quality and uniformity of colloidal nanoparticles.

From the arguments described above, the gold colloids were selected. The last parameter, on which the resonance frequency depends, is the size of nanoparticles [39]. The gold nanoparticles with size in the range of (10–100) nm has their resonance frequencies in the visible spectrum [40]. However, the resonance frequencies are also sensitive to the nanoparticle dielectric environment [41]. Therefore an important task is choosing a proper supporting substrate. In this work, silicon wafers are used.

From above it was shown, the SERS is a method utilized for the enhancement of the Raman signal by plasmonic nanoparticles with size and shape leading to the resonance frequency in the visible range. The SERS method is capable to enhance the intensity of the signal up to $10^6$ [42] compared to the regular Raman signal. Therefore, by using SERS, it is possible to detect much lower concentrations of observed substances. This method is suitable for both basic and applied research.

## 1.3. Application of SERS

SERS is not yet a widespread method used in many branches, because it is difficult to qualitatively understand the exact mechanism of SERS. Until now, SERS is asserted mostly under laboratory conditions. In order to implement this method correctly, it is important to ensure that certain scientific and technological requirements are met prior to practical utilization in everyday life. A continual scientific observation of different probes and substrates opens up new options of applications. The most often used materials for sensing are metals (gold, silver), or special semiconductors as graphene [43, 44]. It needs to be kept in mind that even though the added material enhances the signal, the uniformity of the sample has to remain to provide correct and reproducible signal of sensed substance [44].

One of the essential aspects of SERS method is the fabrication of the substrate. The mutual arrangement of the particles with equal sizes and precision of layout are fundamental. The high sensitivity of SERS method is guaranteed by high density of hot spots[1]. Here an extensive research was done by Nie Kneipp et al. [45], whose enhancing factor rised up to $10^{14}$ in detection of clear molecular structure of a single-molecule. This was possible thanks to the aggregation of cellular compartments to silver and gold nanoclusters, which resulted in an origin of hot spots. If the molecules are positioned precisely close to these hot spots, the detection limit rises and allows to probe and study small biological spieces. Zhang et al. [46] intensively studied new substrates with high density of hot spots in order to detect Raman signal of organic molecules. The intensity was amplified by plasmonic nanostructured metals. In their experiment in 2011, a presence of a big biomolecule of rhodamine 6G (R6G) on wrinkled nanoporous Au films along a wrinkle ridge was successfully detected in a low concentration of $10^{-11}$ M. Later, in the experiment of Lin et al. in 2012 [47], the distinct plasmonic patterns with small molecules were studied. The viruses of different sizes and types were detected on nanostructured Au substrates. Particular Raman shifts then represented their enveloped proteins as specific indicators. Both experiments show, that substrate with suitable properties such as high precision of ordered particles, allows to distinguish the molecules of various sizes and shapes. [48].

For the reasons described above, SERS is an interesting method for various scientific branches. In biochemistry, SERS is often used for detection of DNA, proteins, enzymes, molecules, but also live cells. It is possible to identify biomolecules and determine their structure from the Raman spectrum enhanced by noble-metal nanostructures placed on the substrate. For example, Pallaoro Ch. A. et al. used silver nanorods for SERS detection of low abundance biomolecules or proteins in body fluids [49]. In 2015, the research was focused on monitoring and identification of individual mammalian cells, which continuously flow in a microfluidic channel. The SERS detection sorted out and synthesized cancerous and noncancerous prostate cells and the obtained reliability was one of 100 cells. This experiment was a big step forward for the future's detection and screening of cancer in diagnostics.

In other branches, mobile SERS is used for the analysis and control of purity of the environment. For example in 2011, Li J. et al. [50] studied the sensitivity and selectivity of SERS detection of $As^{3+}$ in order to purify drinking water. Glutathione (GSH)/4-mercaptopyridine (4-MPY)-modified silver nanoparticles were used for binding $As^{3+}$ onto

[1] region of strongly enhanced electromagnetic field

GSH surface from aqueous solution, which was further analyzed by SERS. The enhanced Raman signal of 4-MPY reflected the concentration of $As^{3+}$ in the water. Purification of water also studied Li N. et al. in the most recent experiment in 2017 [51]. They were identifying active polymeric Al species ($Al_{13}$) at solid-liquid interface on $SiO_2$ with silver or gold colloids on the surface. Polymer $Al_{13}$ may optimize the selection of coagulants[2] in the water and regulate pH, basicity or temperature of the water. In the industry, SERS can play an important role in the study of electrochemical systems [52]. Here, this technique provides information about the molecules on the interface of solid-liquid. For example, it is a suitable method for studying the process of corrosion by detecting inhibitors such as benzotriazole [52].

Till now, there are a few applications of SERS in the science such as analytical and physical chemistry, biochemistry, mineralogy, geochemistry and biophysics. SERS is going to be an important instrument not only in pharmacy and medicine, but in the industry and environment as well. In the future, a worldwide spread of the SERS technique is awaited [44].

[2] small particles grouped together in a solution into larger particles

# 2. Graphene in Surface-enhanced Raman spectroscopy

## 2.1. Graphene

Carbon is a well-known element existing in variety of forms. In each form, the carbon atom can be found in a different structure and hybridization (see the Figure 2.1), which determines its chemical and physical properties. The most representative forms of carbon are diamond and graphite. Diamond has face–centered cubic crystal structure of carbons with $sp^3$ hybridization, which is responsible for insulating properties and strength. On the other hand, graphite is conductive and soft thanks to the hexagonal lattice of $sp^2$ hybridized carbon atoms and with weak Van der Waals bonds between the layers. Graphite is composed of recently discovered single-atom wide layers of graphene, which is 2D allotrope with $sp^2$ hybridization.

In the early twenty-first century, great attention was paid to the research of 2D materials. For a long time it was believed 2D materials are too unstable to exist because of thermal fluctuations. But in 2004, in the experiment of Novoselov et al. [1, 2], a single layer of graphite was for the first time isolated and its properties experimentally characterized. The structure, known today as graphene, was fabricated by using an adhesive tape cleaving a monolayer of graphene from bulk graphite. Naturally, as a real sample graphene was discovered to have dramatically different properties compared to other allotropes of carbon. These exceptional properties are for example electronic, such as high electrical conductivity and near ballistic transport [53]. All of them have origin in crystallographic structure of graphene and might be further influenced by the defects such as vacancy, charge disorder or structural distortion [53]

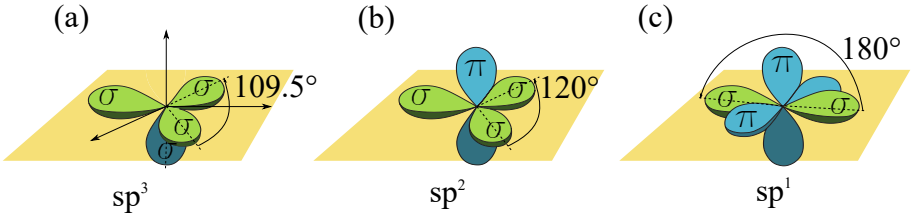


**Figure 2.1:** Comparison of hybridizations: **(a)** $sp^3$ hybridization, **(b)** $sp^2$ hybridization, **(c)** $sp^1$ hybridization. Taken and modified from [54].

### 2.1.1. Structure and electrical properties of graphene

In graphene, carbon atoms are arranged in the hexagonal lattice. The base of the crystallographic structure contains 2 non-equivalent carbon atoms (A and B in the Figure 2.2 (a)). The unit cell is then formed by two overlapped triangles defined by two vectors

$$\mathbf{a_1} = \frac{3}{2}a\mathbf{e_x} + \frac{\sqrt{3}}{2}a\mathbf{e_y}, \tag{2.1}$$

$$\mathbf{a_2} = \frac{3}{2}a\mathbf{e_x} - \frac{\sqrt{3}}{2}a\mathbf{e_y}, \tag{2.2}$$

where $a = 1{,}42$ Å is a distance between carbon atoms, and vectors $\mathbf{e_x} = (1,0,0)$ and $\mathbf{e_y} = (0,1,0)$ are unit vectors of Cartesian coordinate system.

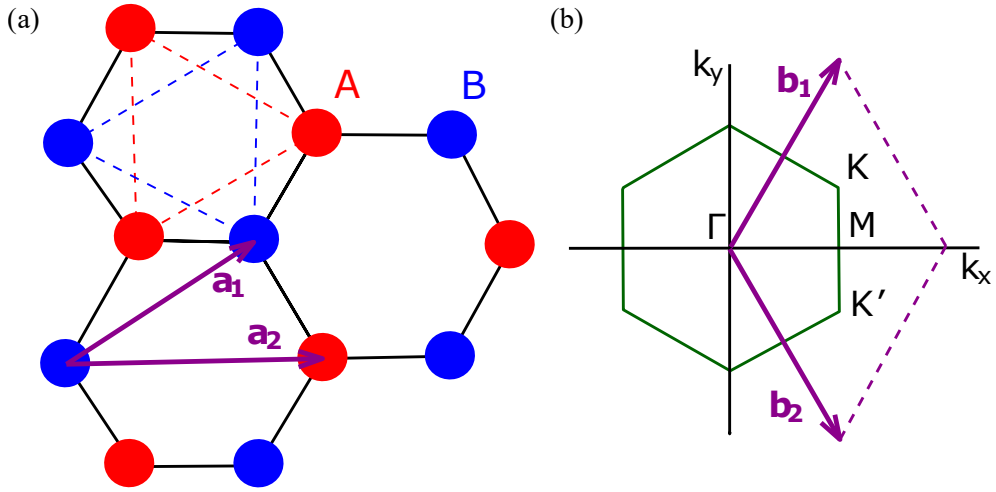


**Figure 2.2:** **(a)** Scheme of hexagonal lattice made of two overlapped triangles of carbons (red and blue), **(b)** reciprocal space of graphene. Taken and modified from [55].

In reciprocal space[1], the vectors of a unit cell are

$$\mathbf{b_1} = 2\pi \frac{\mathbf{a_2} \times \mathbf{e_z}}{|\mathbf{a_1} \times \mathbf{a_2}|} = \frac{2\pi}{3a}\mathbf{e_x} + \frac{2\pi}{\sqrt{3}a}\mathbf{e_y}, \tag{2.3}$$

$$\mathbf{b_2} = 2\pi \frac{\mathbf{e_z} \times \mathbf{a_1}}{|\mathbf{a_1} \times \mathbf{a_2}|} = \frac{2\pi}{3a}\mathbf{e_x} - \frac{2\pi}{\sqrt{3}a}\mathbf{e_y}, \tag{2.4}$$

where $\mathbf{b_1}$ and $\mathbf{b_2}$ are basal vectors of reciprocal lattice and $\mathbf{e_z} = (0,0,1)$ is a unit vector of Cartesian coordinate system. The reciprocal space with marked Brillouine zone is shown in the Figure 2.2 (b).

A single carbon has 4 electrons, usually all are used for bonds. In case of graphene, due to $sp^2$ hybridization, 3 electrons make $\sigma$-bonds with the carbon neighbors. Through $\sigma$-bonding, a strong covalent bond in the grid plane of orbitals 2s, $2p_x$ and $2p_y$ is produced. Thanks to the strength of the covalent bonds, graphene is one of the strongest materials in the world. The values of Young's modulus (1 TPa) and intrinsic strength (130 GPa) are respectively 5 and 20 times greater than those of steel, but with just a third of steel's weight [56–58]. The last electron from $p_z$ orbital, which is perpendicular to the plane of the crystal, participates in the $\pi$-bond responsible for high thermal and electrical conductivity [59].

The electronic structure of graphene can be described by using an orthogonal nearest-neighbor tight-binding approximation [60]. By using this model, the band structure of graphene exhibits the symmetry of conduction and valence band with respect to the Fermi energy. The energy dispersion relation is defined by Schrödinger equation

$$E(\mathbf{k_x},\mathbf{k_y}) = \pm\gamma_1 \sqrt{1 + 4\cos\left(\frac{\sqrt{3}a\mathbf{k_y}}{2}\right)\cos\left(\frac{a\mathbf{k_x}}{2}\right) + 4\cos^2\left(\frac{\sqrt{3}a\mathbf{k_y}}{2}\right)}, \tag{2.5}$$

[1] plane perpendicular to the plane of a crystal

where $\mathbf{k_x}$, $\mathbf{k_y}$ are the components of the $\mathbf{k}$ vector in the first Brillouine zone and $\gamma_1$ represents the hopping energy. $(+)$ expresses the conduction band $\pi^*$ and $(-)$ valence band $\pi$ [61]. Both bands meet in the charge neutrality point, so called Dirac point (0 eV), see diagram in the Figure 2.3 [62]. Therefore, graphene is a zero-band gap semiconductor.

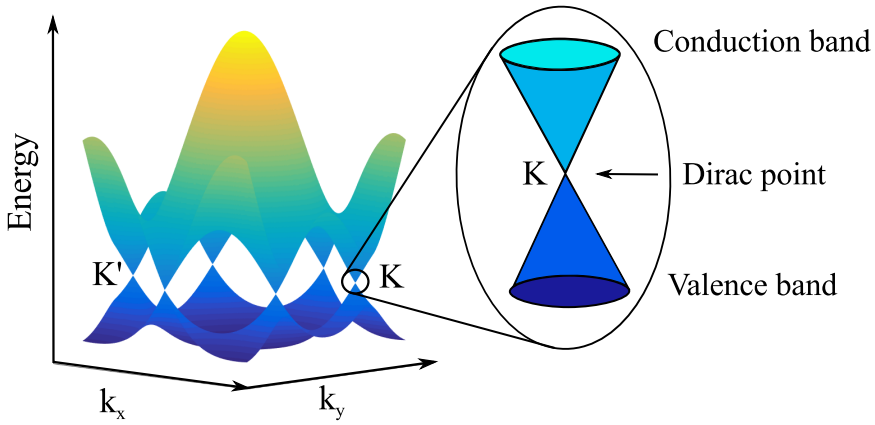


**Figure 2.3:** Graph of energy dispersion relation in graphene. Taken and modified from [63].

### 2.1.2. Raman spectrum of graphene

Raman spectroscopy is used with the advantage of fast qualitative analysis of graphene layers. First of all, Raman spectroscopy of graphene can provide the information about graphene's thickness with a layer resolution. Measured fingerprints of graphene allow to examine the quality of the sample by detecting the defects and impurities and to determine the tension caused by deformation. Also, it is possible to estimate the concentration of charge carriers and to monitor the doping of graphene [64].

Characteristic Raman spectrum of graphene contains three significant peaks (G, 2D and D) in the field of $(1300 - 3000)$ cm$^{-1}$. More specific location is shown in the Figure 2.4 (a). The position and the height of these peaks reflect the properties of graphene. Mutual ratio of the amplitudes of G–peak and 2D–peak dictates the amount of layers. For example, in the spectrum of graphene (Figure 2.4 (a)), 2D–peak is two times higher than G–peak, which signalizes, that the measured place of the sample is a monolayer. The more layers the sample contains, the lower 2D–peak and higher G–peak is (demonstrated in the Figure 2.4 (b)) [13, 65]. The last peak, D–peak, does not occur in impurity free graphene. It is activated due to the presence of defects in the crystallographic structure. So the sample in Figure 2.4 (a) is homogeneous without impurities (red drawn D–peak is only schematical).

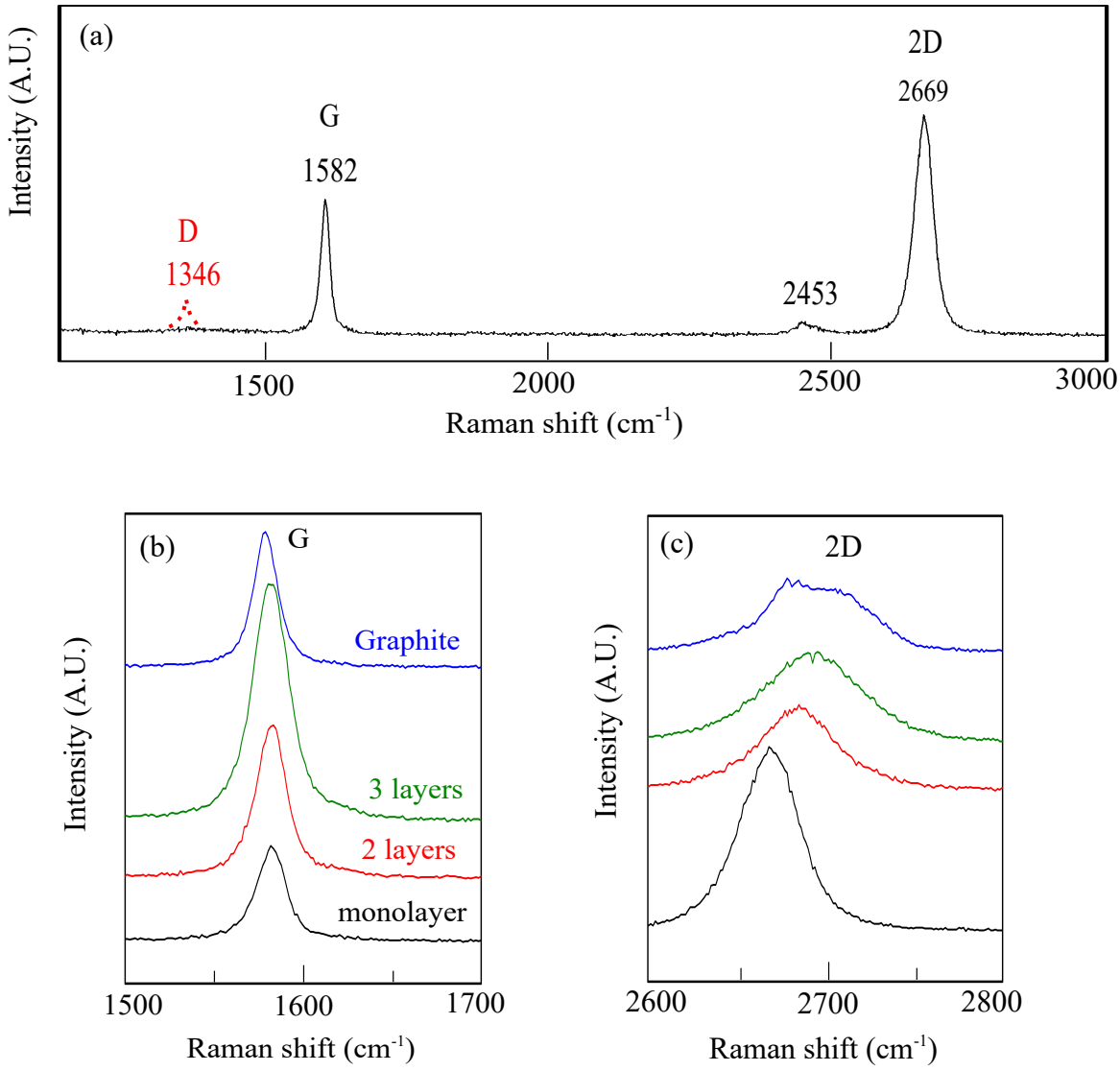


**Figure 2.4:** **(a)** Raman spectrum of graphene by Stokes scattering with 2 characteristic peaks. The red D–peak occurs in defected graphene. Intensity and position of **(b)** G–peak and **(c)** 2D–peak with respect to the amount of layers.

## 2.2. Utilization of graphene in SERS

There are great expectations for future utilization of graphene in commercial sphere. Its very low thickness and transparency is favorable for use in flexible and organic light-emitting diode displays, or for solar cells [43]. Further, electronic properties make graphene a great candidate to partially replace silicon in semiconductor industry. It has already been tested in transistors, which could be made with very thin and short channel leading to higher switching speed [66].

Recently, graphene was considered as a suitable material for energy storing [62]. Here, graphene can be adapted as active or passive medium in lithium-ion batteries and electro-

chemical capacitors [67]. The specific electron and phonon structure of graphene opened the research in several branches and also the tasks of clarifying the fundamental features of SERS mechanism. Here, graphene was used in different areas of interest.

Firstly, graphene was used as a probe for studying SERS mechanism. An important criterion, essential for the enhancement of Raman intensity, is to use the appropriate substrate. Measured Raman spectrum of graphene is highly sensitive to the shape and size of inspected plasmonic nanostructures and enables to study their SERS activity [43].

Further, graphene can be used as a SERS substrate. However, the dominant electromagnetic enhancement is absent as for all semiconductors and transition metals [68]. Only noble metal surfaces enhance electromagnetically due to which the SERS sensitivity is upheld. The SERS activity of graphene was for the first time observed by Ling et al. [69] who called this phenomena as graphene-enhanced Raman scattering (GERS). They observed, that the remaining organic residues originating from the mechanical exfoliation are easier to be detected on graphene than on surrounding $SiO_2$ surface. They attributed the enhancement of their Raman signal to SERS activity through the chemical mechanism. After this experiment, the organic dyes started to be intentionally used to estimate graphene SERS properties. Thanks to the flat surface of graphene, GERS later turned up to be well utilized for probing and controlling molecular orientation during the measurement [70]. In another experiment of Ling et al. [70], the Raman intensity of CuPc monolayer dependent on the rising temperature was studied. It was proven, that besides the higher molecular sublimation with the temperature, the orientation of molecules assembled on the substrate is crucial for their GERS detection.

Even though graphene substrates enhance chemically with much lower factor, there is one big advantage – fluorescence quenching. Fluorescence quenching was demonstrated by Xie et al. [3], who showed, that the fluorescence signal of rhodamine and protoporphyrin dyes is much less present on graphene than on $SiO_2$ substrate. This also enables easier detection of the Raman signal. For fluorescence quenching properties, graphene seems to be suitable for example for utilization in ultraviolet resonance Raman spectroscopy (UV-RRS) [4] or for time-resolved Raman detection [71]. By UV-RRS DNA and RNA bases were studied with excitation Ar ion laser. Here, the intensity of fluorescence had to be lowered to minimize the decomposition of nucleotide-containing biomolecules. Other advanced properties of graphene useful for biosensing are biocompatibility and chemical stability. The molecules assembled directly on metal surfaces are easy to interact with the surface and to decompose compared to the molecules, whose contact with metal is isolated by graphene [72].

# 3. Experimental part

The main goal of this bachelor's thesis is fabrication of graphene/metal heterostructures and their utilization as a sensing platform in surface-enhanced Raman spectroscopy. The structures are fabricated by a selective deposition of gold colloidal nanoparticles (AuNPs[1]) on desired substrate and subsequently covered by graphene. The selective deposition is attained by irradiation of specific sites of the sample, which changes the surface termination and the gold colloids stick to these sites with different probability. Main effort is focused on establishing easy and especially well reproducible process of fabrication with equal properties on the output. The fabricated surface includes parts with different concentrations of AuNPs. The goal is to prepare on the same substrate areas with, and without AuNPs. Then it is possible to examine the strength of Raman signal of graphene in dependence on the presence of AuNPs. Therefore, the impact of added AuNPs and the potential utilization in SERS is immediately visible.

## 3.1. Fabrication of graphene/metal heterostructures for SERS

The substrates used for graphene/metal heterostructures are silicon wafers with native oxide or with 285 nm thick layer of $SiO_2$ (further only Si and $SiO_2$ respectively). The most important substrate properties for the experiment are summarized in the Table 3.1 and its benefits are further studied in the experiment.

| Substrate | Si | $SiO_2$ |
|---|---|---|
| Manufacturer | Siltronix CZ | on Semiconductor CZ |
| Orientation | $< 111 > \pm 0.05°$ | $< 100 > \pm 0.05°$ |
| Thickness (µm) | $375 \pm 25$ | $525 \pm 15$ |
| Resistivity (Ωcm) | $0.01 - 0.02$ | $0.5777 - 0.6013$ |
| Type/Dop. | N-Ph | N-Ph |
| Final bath* | isopropyl alcohol | ultraclean water |
| Termination* | –H, $–CH_x$, –OH | –OH |
| Surface* | more hydrophobic | less hydrophobic |

**Table 3.1:** Overview of important properties of two types of silicon wafers used in the experiment for AuNPs self-assembly. The data marked by (*) are taken from [73].

The fabrication can be divided into three parts, see the scheme in the Figure 3.1. At first (a), the specific sites of the sample are irradiated by an electron beam (e–beam) in the scanning electron microscope (SEM). Secondly (b), the sample is inserted for two hours into a colloidal solution of AuNPs in order to adhere the particles onto the substrate. In the last step (c), the substrate with gold colloids is overlaid by a monolayer of graphene.

[1] s represents the size of nanoparticles in nanometers

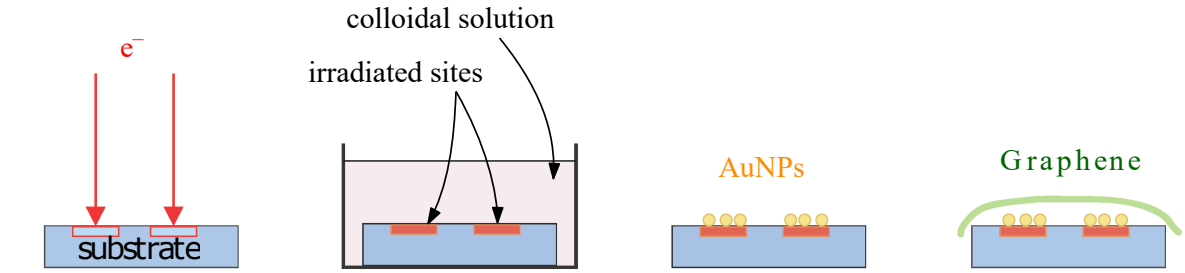


**Figure 3.1:** Schematic fabrication of graphene/metal heterostructures in three steps. **(a)** The irradiation of specific sites of the sample. **(b)** Selective deposition of AuNPs on the substrate. **(c)** Graphene overlays the prepared sample.

### 3.1.1. Deposition of gold colloids on Si-substrate with native oxide on the surface

The deposition of gold colloids depends on a number of aspects. The fact whether a colloid adheres onto a bare (non-irradiated) substrate or not depends on the surface termination of both substrate and AuNPs in the colloidal solution. The adhesion properties can be tuned by e-beam prepatterning of the substrate surface and by hydrogen fluoride (HF) modification of AuNPs solution. It is very important to find a good combination of both transformations together.

The surface of Si–substrate in ambient conditions is predominantly terminated by –OH groups and the AuNPs colloids in the carrying solution by $COO^-$ groups. When the substrate is inserted into AuNPs solution, the surface becomes also negatively charged due to deprotonation (–OH $\rightarrow$ $–O^-$). It is necessary to change one of the charges to positive, otherwise no particle would get attached to the surface. For this reason, different amount of hydrofluoric acid[2] is added to AuNPs solution to achieve their adhesion. By making the solution more acidic, the deprotonation is prevented, or even the charge of Si surface turns to positive (formation of $–OH^{2+}$ instead of $–O^-$). To control the adhesion of Si-substrate, the 2% diluted HF was added into AuNPs solution. The adhesion ability in dependence on the amount of added HF is shown in the Figure 3.2 for AuNP20. The selective deposition of AuNPs can be achieved on e–beam prepatterned Si–substrate. E–beam irradiation of specific sites causes local changes of surface termination groups. The Figure 3.3 (I.) schematically shows a bare substrate, (II.) an irradiation pattern with different electron doses (e–doses) and (III.) a substrate after the exposition. In dependence on e–dose, AuNPs adhere with different probability on sample surface. It is possible to attain (a) positive or (b) negative deposition. A small dose leads to the positive deposition of AuNPs. The initial surface groups such as –H and $–CH_x$ of a bare substrate are mostly substituted by –OH groups, which are more adhesive for AuNPs. On the other hand, the negative deposition occurs, if the surface is irradiated by a high dose. The surface gets contaminated by carbon, which is unfavorable for AuNPs.

[2]HF diluted by water

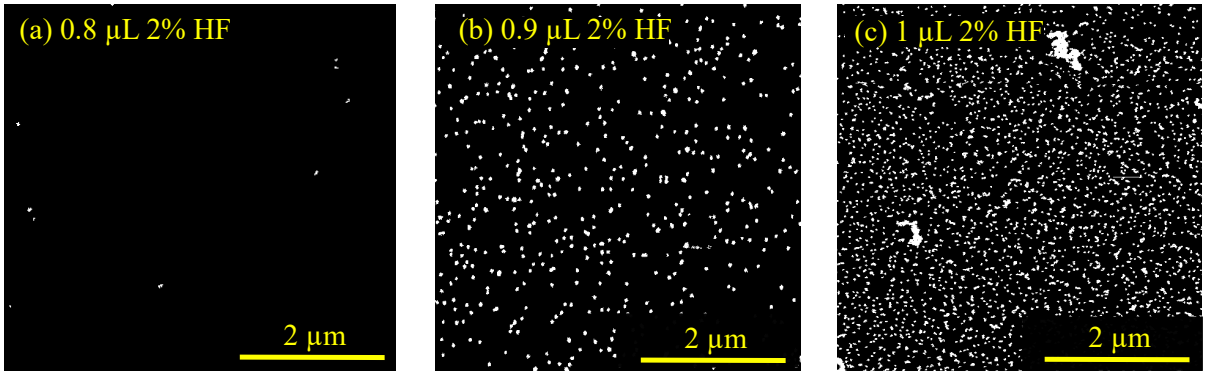


**Figure 3.2:** The AuNP20 adhered on Si–surface in dependence of 2% HF added into 400 µL AuNP20 solution. Presented SEM images show the results for three amounts of added HF: **(a)** 0.8 µL 2% HF, **(b)** 0.9 µL 2% HF, **(c)** 1 µL 2% HF.

For better understanding and control of AuNPs deposition, the surface potential (SP) measurements on e–beam prepatterned samples were carried out by Kelvin Probe Force Microscope (KPFM). The SP characterization of irradiated parts was done depending on the e–dose used during the patterning. The Figure 3.4 shows an evolution of SP versus e–dose (I.) and a correlation of the obtained SP data to the concentration of attached AuNPs on irradiated sites gained from SEM (II.).

The graph in the Figure 3.4 (I.) shows, that the most successful e–dose for positive deposition is 600 µC/cm$^2$. At this dose, the density of adhered AuNPs reaches the highest value (87 AuNPs/cm$^2$). The comparison of the SP of irradiated sites to adhered AuNPs is shown in the Figure 3.4 (a). By using such a low e–dose as 600 µC/cm$^2$, it was possible to prepare several (100 × 100) µm$^2$ patterns. The (5 × 5) µm$^2$ irradiated areas were 5 µm apart as shown in the Figure 3.5 (a). To obtain the positive deposition, the sample was inserted into the solution made of 400 µL of AuNP20 and 0.9 µL of 2% HF. However, AuNP20 did not adhere in this attempt with the high concentration difference of AuNPs on desired sites. Generally, the positive deposition was found to be hardly reproducible. Better option is the negative deposition. With lower and higher e–dose such as 100 µC/cm$^2$ or 1000 µC/cm$^2$, the AuNP20 density declined (see the Figure 3.4 (c)), so the influence of irradiation on AuNP20 adhesion to the substrate surface was not observed. With e–dose 2500 µC/cm$^2$ or higher, the AuNPs density was low and have not changed (Figure 3.4 (b)). In the Figure 3.5 (b), the sample patterns were exposed to e–dose of 2500 µC/cm$^2$. The diverse concentrations of AuNP20 attached on irradiated and non-irradiated sites are evident.

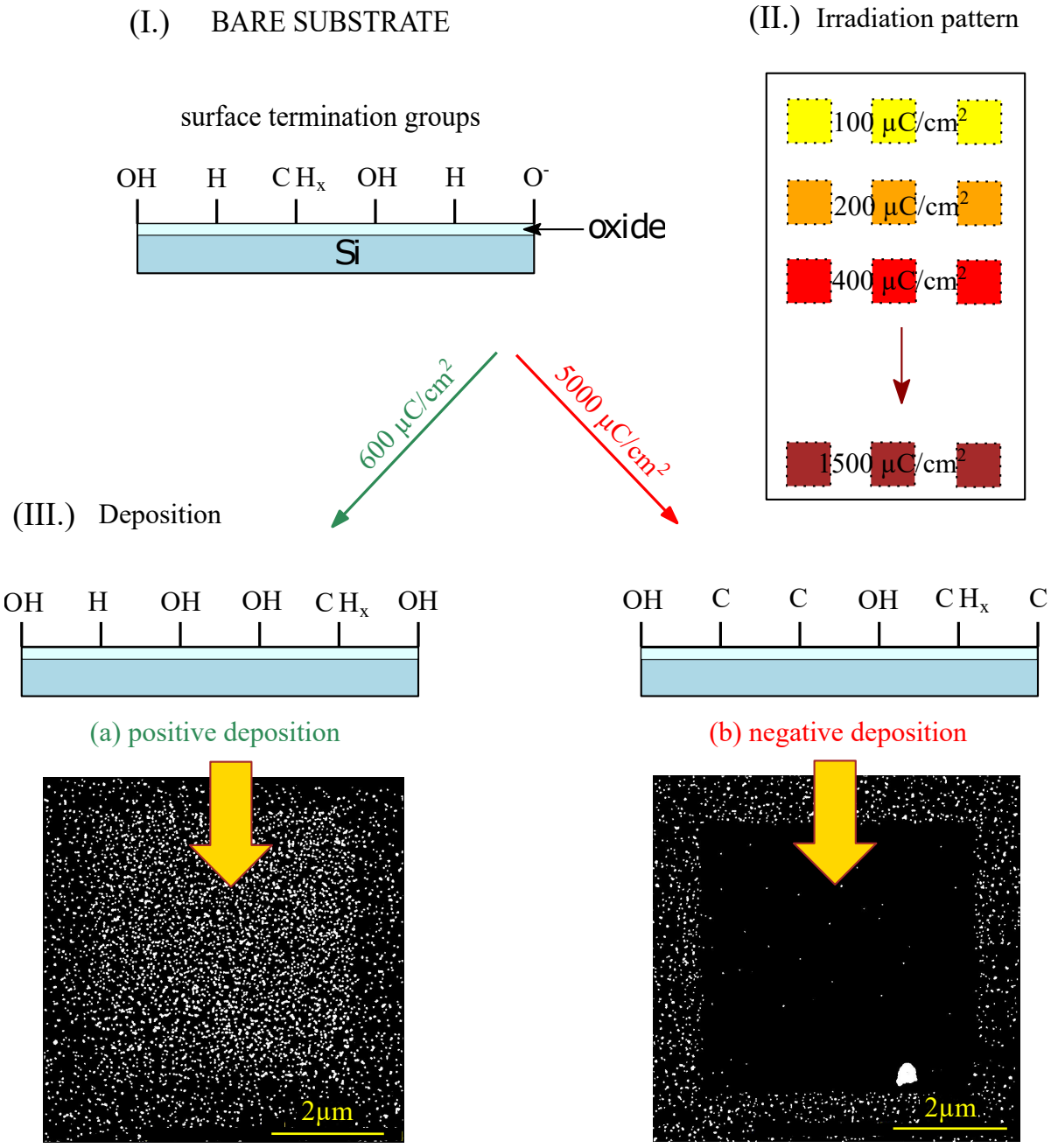


**Figure 3.3:** Scheme of the effect of irradiation on surface termination. **(I.)** the surface termination of a bare substrate. **(II.)** The irradiation pattern of distinct doses on one sample. **(III.)** The change of surface termination of irradiated squares for deposition **(a)** AuNP20 positive, **(b)** AuNP20 negative. The surface termination taken and modified from [74].

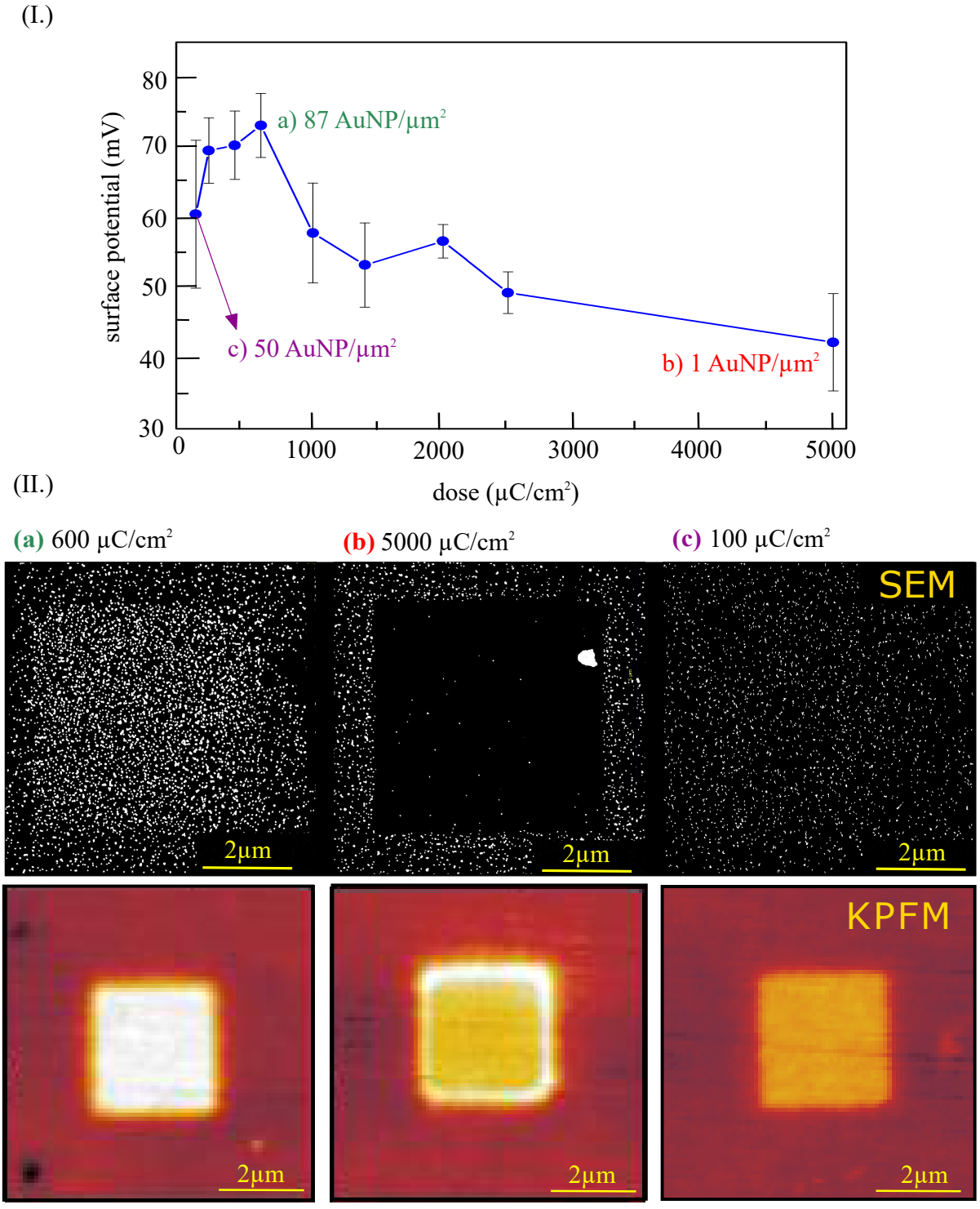


**Figure 3.4:** The dependence of surface potential and amount of AuNP20 on the irradiation. **(I.)** The graph shows surface potential dependent on the dose of irradiation with mentioned amount of AuNP20 (adhered on the substrate). **(II.)** KPFM images of irradiated sites in comparison to SEM images after inserting to the solution with 400 µL of AuNP20 and 0.9 µL of 2% HF: **(a)** positive deposition, **(b)** negative deposition, **(c)** equal behavior on the irradiated and non-irradiated site.

(a) positive deposition - 600 µC/cm2

(b) negative deposition - 2500 µC/cm$^2$

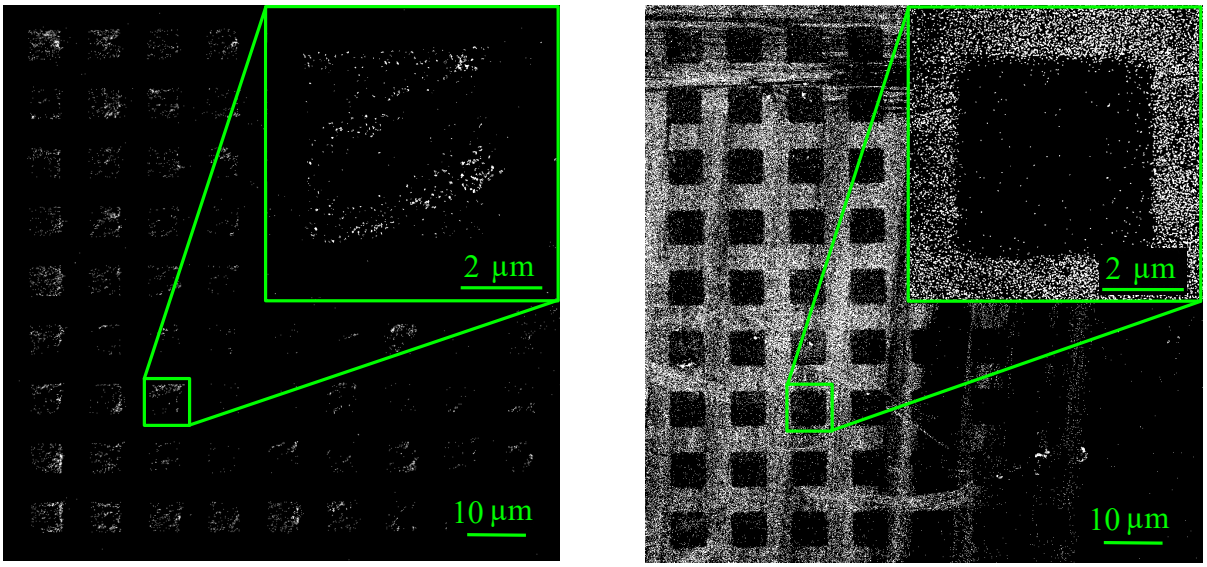


**Figure 3.5:** The field of selective deposition of AuNP20 on Si–substrate in SEM with detailed square: **(a)** positive deposition, **(b)** negative deposition.

(a) electron microscope

(b) optical microscope

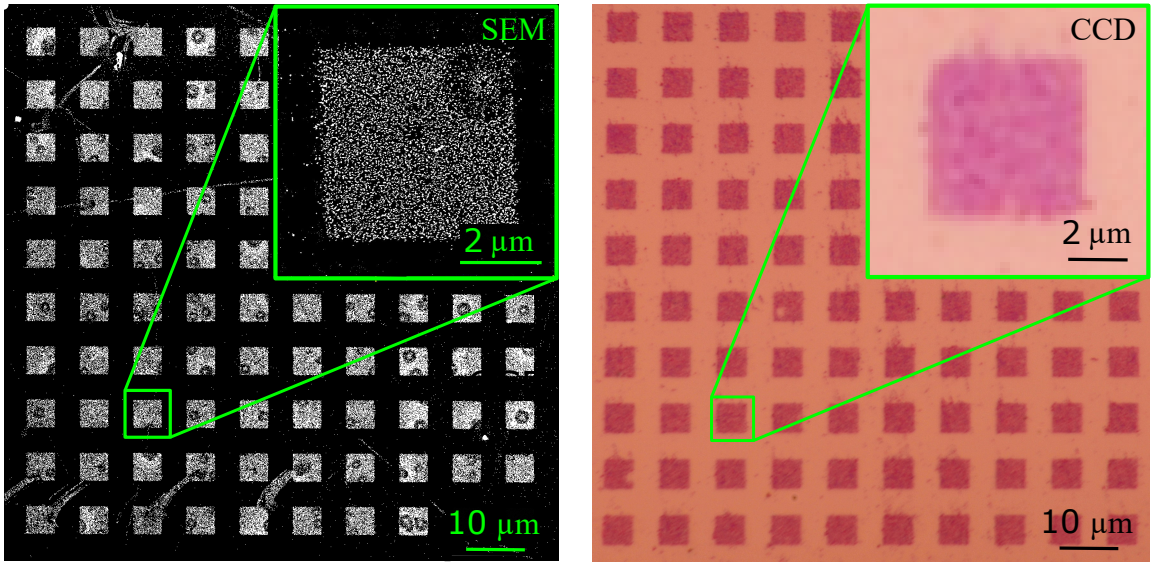


**Figure 3.6:** The field of positive deposition of AuNP20 on $SiO_2$ with detailed square: **(a)** in SEM, **(b)** in the optical microscope.

### 3.1.2. Deposition of gold colloids on silicon substrate with 285 nm thick layer of $SiO_2$

The deposition on Si-wafer with 285 nm thick layer of $SiO_2$ (further only $SiO_2$) was carried out in the same way as on Si-substrate with native oxide as it was described in the section 3.1.1. However, the deposition has shown much better feasibility and reproducibility mainly due to lower sensitivity of AuNPs adhesion towards HF concentration in colloidal solution. It is less susceptible to the pH error of the solution made by adding a slightly different amount of HF, so AuNPs are placed more easily on desired sites. After a selective deposition of AuNPs, a thick layer of $SiO_2$ benefit to acceptable visibility of AuNPs squares in the optical microscope (the photo from a camera in the Figure 3.6 (b)).

To achieve the AuNPs adhesion on $SiO_2$ substrate, it was necessary to make the solution more acidic compared to Si–substrate with native oxide. The Figure 3.6 (a) shows AuNP20 positive deposition in SEM and (b) in the optical microscope. A $(100 \times 100)$ µm$^2$ pattern of $(10 \times 10)$ squares 5 µm apart was irradiated by e–dose of 250 µC/cm$^2$. After inserting the sample into AuNP20 solution made of 400 µL AuNP20 and 2.4 µL of 2% HF, most of AuNP20 were adhered on the irradiated sites.

Similar results were obtained for other sizes of AuNPs colloids. The parameters of positive deposition for different AuNPs sizes are summarized in the Table 3.2.

| size (nm) | e–dose (µC/cm$^2$) | AuNPs solution (µL) |
|---|---|---|
| 10 | 250 | 400 AuNP10 + 1.0 2% HF |
| 20 | 250 | 400 AuNP20 + 2.4 2% HF |
| 40 | 250 | 400 AuNP40 + 2.4 2% HF |
| 80 | 400 | 400 AuNP80 + 5.0 2% HF |

**Table 3.2:** Parameters of positive deposition for different sizes of AuNPs colloids.

### 3.1.3. Fabrication of graphene and its transfer on Au colloids

Graphene used in this experiment is grown by chemical vapor deposition (CVD[3]). In this process, a layer of graphene is formed on the surface of catalyst (cooper foil) during the pyrolitic decomposition of hydrocarbons ($CH_4$). Graphene is then transferred from the surface of cooper foil to the desired substrate. A conventional wet polymer-based transfer of graphene is accomplished by covering a layer of graphene with poly-methyl methacrylate (PMMA), see the scheme in the Figure 3.7. The cooper foil is etched in etching solution and the layer of PMMA with graphene is cleaned in distilled water and HCl. The layer is then lifted up from distilled water by substrate with AuNPs. After slow drying for one hour, the last process is to dissolve the layer of PMMA in acetone and leave a monolayer of graphene adhered on the substrate.

[3]Graphene was fabricated by Ing. Pavel Procházka in CVD chamber at the Institute of Physical Engineering.

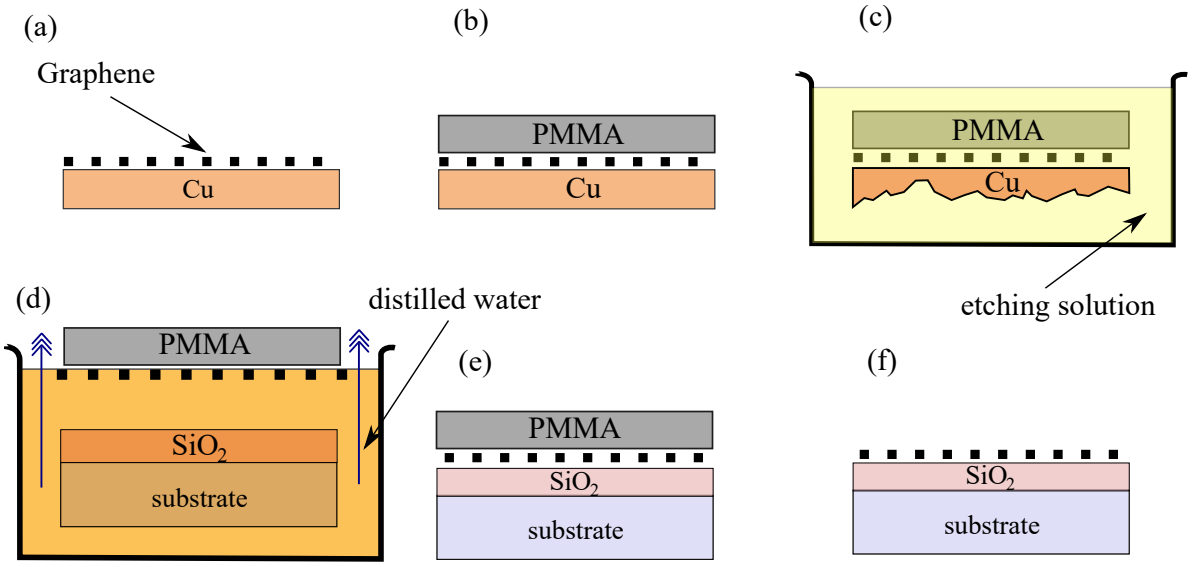


**Figure 3.7:** Scheme of the procedure of the conventional wet transfer of the graphene layer on non-conductive substrate using PMMA. **(a)** Graphene is prepared on Cu foil by CVD. **(b)** Surface of graphene is covered by a thin layer of PMMA. **(c)** the structure is inserted into a solution to etch the Cu foil of. **(d)** Cu foil is etched and the layer of graphene/PMMA floats on the solution surface. **(e)** Graphene is picked up by $SiO_2$. **(f)** PMMA is dissolved. The scheme was taken and modified from [75].

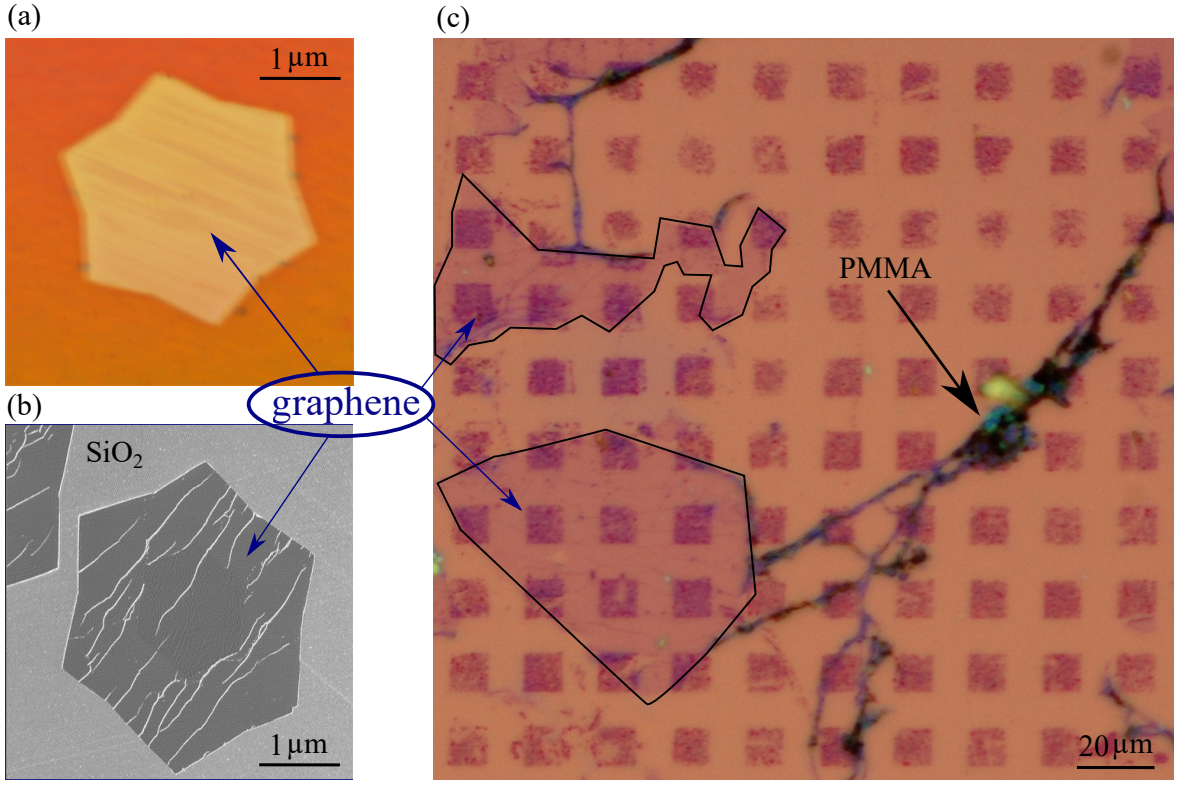


**Figure 3.8:** A monocrystal of graphene **(a)** on Cu–foil in an optical microscope and **(b)** on $SiO_2$ in SEM. **(c)** Torn graphene monolayer on $SiO_2$ in SEM.

The Figure 3.8 shows (a) an optical image of a graphene monocrystal on Cu foil and (b) a SEM image on $SiO_2$. After the transfer, the fabricated heterostructures were inspected under the optical microscope. As it is visible in the Figure 3.8 (c), the graphene monolayer usually does not overlay all AuNPs structures. Therefore, the selective deposition realized on big AuNPs/$SiO_2$ patterns benefits the graphene's examination. The morphology of graphene/metal heterostructures were studied by Atomic Force Microscopy (AFM) and Scanning Electron Microscopy (SEM) on the fully covered graphene areas. The Figure 3.9 shows (a) the SEM image and (b), (c) AFM images of graphene/AuNP80 on $SiO_2$. As it can be seen, graphene does not completely veil the AuNP80 structures and is partially suspended between the colloids in form of graphene membrane (see (a), (b) details). The suspension of graphene is further nicely demonstrated in the image (c) showing the 3D topography overlaid with colored map, which represents the local surface deformation. The bright colored areas correspond to the sites with suspended graphene, where the surface deformation is higher. This measurement was carried out using the peak–force tapping mode of Icon Dimension AFM.

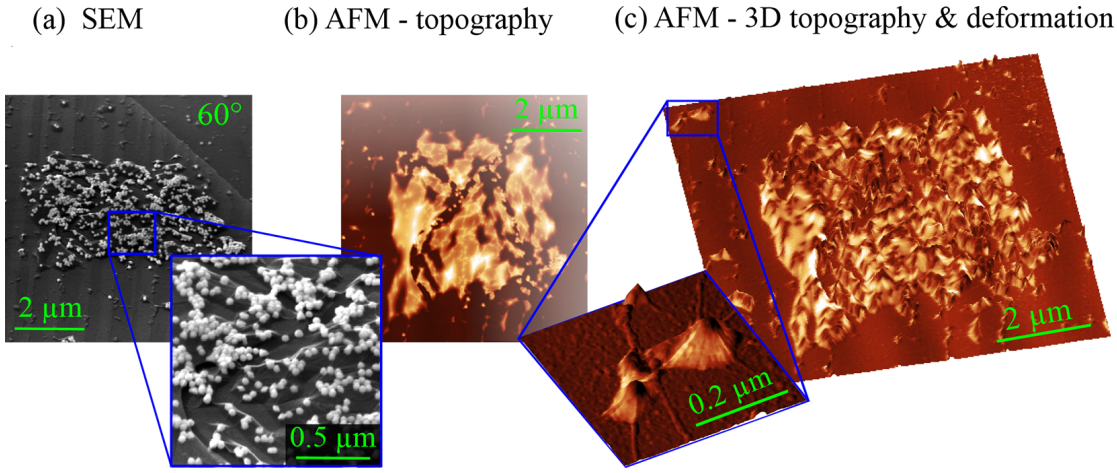


**Figure 3.9:** Characterization of graphene/AuNP80/$SiO_2$ layers. **(a)** SEM image of graphene membrane on AuNP80. **(b)** AFM image of topography on the substrate. **(c)** 3D topography overlaid with colored map representing the surface deformation. The brighter color indicates higher deformation.

## 3.2. Raman spectroscopy on graphene/AuNPs heterostructures

The Raman spectroscopy characterization of graphene/metal heterostructures focuses on the influence of AuNPs presence on Raman spectrum of graphene. For now, graphene takes a role of a probe thanks to the well known Raman spectrum. The aim is to observe the enhancement of G and 2D–peak (or occurrence of D–peak) in dependence on the size of AuNPs. The Raman spectroscopy measurements were carried out by micro–Raman spectroscope Ntegra Solaris using 100× objective lens and 532 nm excitation laser with power of 3.5 mW. The exposition time for single spectrum was 1 s. The Figure 3.10 (a) shows a comparison of graphene/metal heterostructures with AuNP20 and

(b) with AuNP40. Different behavior was observed with respect to the size of AuNPs. The black line represents Raman spectrum of graphene on $SiO_2$, the red line enhanced Raman signal of graphene by AuNPs on $SiO_2$ and the red dashed line enhanced Raman signal of graphene after the subtraction of Au fluorescence.

In the Figure 3.10 it is evident, that the assembled graphene in both situations was a monolayer (from the ratio of 2D and G–peak in Raman spectrum of graphene). In case of graphene on 20 nm AuNPs (Figure 3.10 (a)), the intensity of peaks homogeneously raised approximately 2.5 times. The increased intensity might be explained by the enhancement of Raman scattering due to the presence of gold nanoparticles. However, in case of graphene on AuNP40 (Figure 3.10 (b)), the situation is different. The 2D and G–peak became slightly broadened and their ratio does not correspond to the one of the graphene monolayer. Further, D–peak occured in the spectrum of graphene on AuNP40, even though it did not exist in AuNP40 free surroundings. This effect was even more obvious for heterostructures with 80 nm AuNPs, where Raman spectrum of graphene was almost not readable. This might be explained by higher adsorption of laser light, which leads to the damage of graphene because of heating.

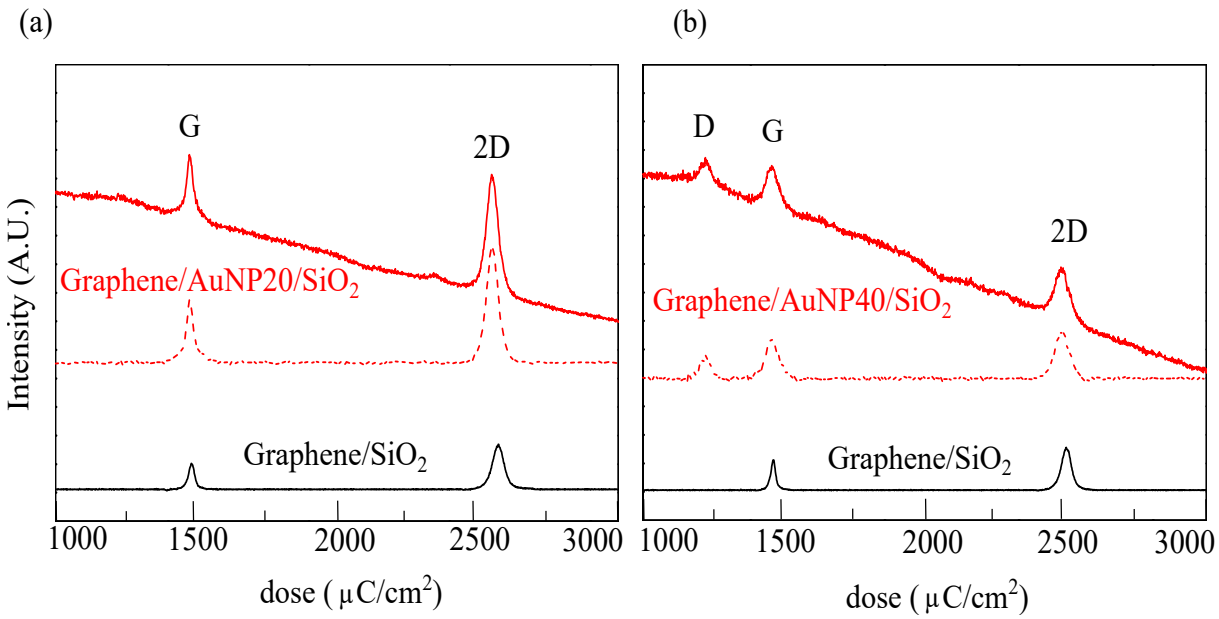


**Figure 3.10:** Raman spectrum of graphene on $SiO_2$ excited by laser $\lambda_0 = 532$ nm. Black line represents graphene/$SiO_2$ layer, red line graphene/AuNPs/$SiO_2$ layer and red dashed line graphene/$SiO_2$ layer after the subtraction of Au fluorescence. The characteristics were measured on the sample with positive deposition of **(a)** AuNP20, **(b)** AuNP40.

## 3.3. SERS study of rhodamine on graphene/AuNPs heterostructures

In the previous section 3.2, the use of AuNPs was confirmed as a good material for enhancing Raman spectrum of graphene. Here, the main goal was to test the feasibility of graphene/metal heterostructures for biosensing. For this purpose, rhodamine 6G (R6G) was used as a test biomolecule. Different concentrations of R6G were applied on the sample by drop casting. First, a small droplet of solution containing R6G was placed by a pipette onto the substrate. After 30 minutes, the droplet was washed away by distilled water and the sample was dried by nitrogen flow. The detection of R6G fluorescence signal was used for verification, whether the R6G molecules were successfully deposited in all areas of interest.

The Raman signal of R6G was measured and compared in distinct areas of the sample. The SERS experiment was carried out with the same system as described in the previous section 3.2. Only the laser power was lowered to 0.2 mW and the exposition time was 10 s. The reason for lowering the power of the laser was to avoid the heat-induced damage and decomposition of R6G molecules. The graphs in the Figure 3.11 show Raman spectrum of R6G (after the subtraction of R6G fluorescence) measured directly on $SiO_2$ (black line), on graphene/$SiO_2$ (red line), on AuNPs/$SiO_2$ (green line) and on graphene overlaid AuNPs on $SiO_2$ (blue line). The used graphene/metal heterostructures were positive deposition of AuNP20 (a), (c), (e) and AuNP40 (b), (d), (f) covered by graphene. The fabrication was in-depth described in sections 3.1.2 and 3.1.3. The examination of low R6G concentrations was carried out on 1 $\mu$M R6G (a), (b), 0.2 $\mu$M R6G (c), (d) and 0.02 $\mu$M R6G (e), (f).

In all graphs in the Figure 3.11, it can be seen, that the spectrum of R6G on $SiO_2$ was not measurable. In case of graphene/$SiO_2$, weak sign of R6G Raman spectrum was visible only for concentration of 1 $\mu$M (a), (b). At this concentration, the Raman signal on graphene/AuNPs/$SiO_2$ and on AuNPs/$SiO_2$ was clearly visible. The signal seemed to be the strongest in case of bare AuNPs without graphene ((a), (b) – green line). For the concentration 0.2 $\mu$M R6G (c), (d), the intensity of R6G peaks decreased for both, graphene veiled AuNPs and bare AuNPs, but still the signal remains stronger in case of 40 nm particles (d). When the R6G concentration was lowered down to 0.02 $\mu$M R6G (e), (f), the low intensity of the Raman signal of R6G was detectable only in case of AuNP40/$SiO_2$ and graphene/AuNP40/$SiO_2$ (f – green and blue line respectively).

From the presented data, the role of graphene in the enhancement of R6G signal is not evident. Nevertheless, the advantage of graphene is in weakening of R6G fluorescence. Thanks to this quenching, the Raman signal of R6G was more easily separated from the fluorescence background.

### 3.3. SERS STUDY OF RHODAMINE ON GRAPHENE/AUNPS HETEROSTRUCTURES

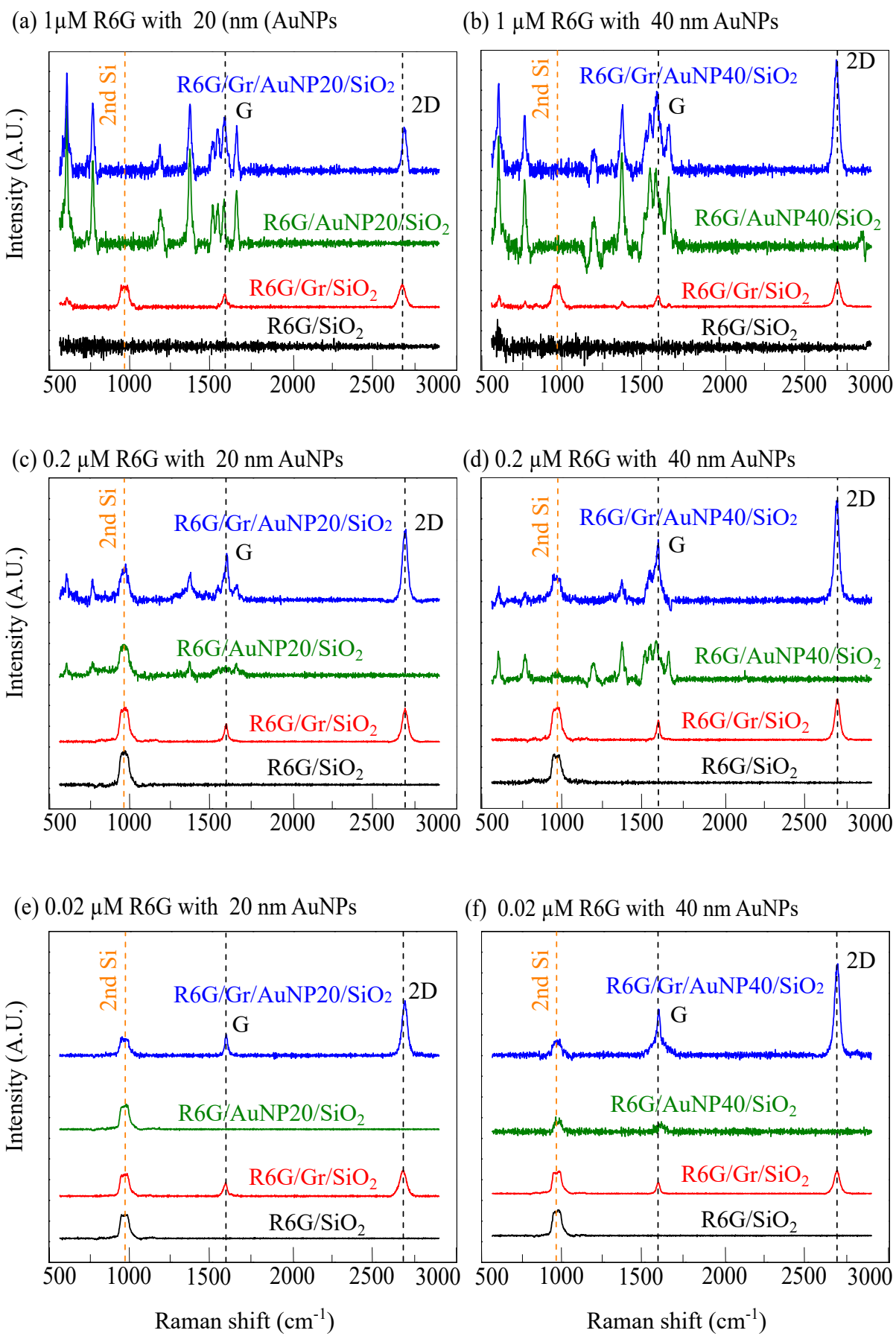


**Figure 3.11:** Raman spectrum of R6G with diverse concentrations on different layers.

# Conclusion

This bachelor's thesis mainly focused on the fabrication of graphene/metal heterostructures. The characterization and the examination of prepared structures determined, if the structures are suitable for future application in biosensing. The thesis is divided into three parts, where the first two sections are theoretical and the last one summarizes the experimental results.

The first section of the thesis contains a brief introduction to Raman spectroscopy and to the mechanism of SERS. Further, the prospective utilization of SERS in the future was discussed. The review shows, that the SERS technique is also feasible with recently discovered graphene. Graphene, as a new 2D material described in the second section, improves the detection limits of measurements. This enables to study molecular structure of species at very low concentrations.

The experimental part begins with fabrication of graphene/metal heterostructures. The substrate used as a platform was a silicon wafer with native oxide or with 285 nm thick layer of thermal $SiO_2$. The first step in the fabrication process was selective deposition of colloidal AuNPs on e–beam prepatterned substrate. The used sizes of AuNPs were 10, 20, 40 and 80 nm. Because of unstable AuNPs deposition on Si-substrate, the most experiments were done on $SiO_2$. The deposited structures were overlaid by graphene and examined for possible application in biosensing. The characterization of prepared heterostructures was carried out by SEM, KPFM and AFM. KPFM was used during the fabrication process to study the influence of e–beam irradiation on surface potential and further AuNPs adhesion behavior. AFM and SEM were utilized to observe the morphology of graphene overlaid AuNPs. Then the Raman spectroscopy was used to study the SERS effect of different sizes of AuNPs on the intensity of Raman spectrum. In this experiment, the Raman signal of graphene in heterostructures with AuNP20 was two times higher compared to graphene on the bare substrate. On the other hand, such an enhancement was not observed on AuNP40, but the D–peak occured. This result also emerged on AuNP80, where the changes in Raman spectrum were even more obvious. Possibly, the intensity of excitation laser was too high leading to the damage of graphene as a result of heating. If the excitation laser were lowered, the graphene monolayer would likely remain undamaged and allow to detect clear enhanced Raman spectrum without defects.

The suitability of graphene/AuNPs/$SiO_2$ heterostructures in SERS biosensing was tested upon a detection of molecule of R6G with high fluorescence. The fluorescence signal was used to verify the presence of biomolecule all over the inspected sample surface. The aim was to find the lowest concentration, where Raman spectrum of R6G was still measurable. For now, the lowest concentration of R6G measured in this experiment was 0.02 $\mu$M of R6G on heterostructures with AuNP40.

Future goal of this research is to study the effect of different AuNPs sizes on the Raman signal, or surface modifications such as annealing to gain higher adhesion of graphene to AuNPs colloids. In addition to graphene, a potential utilization of other 2D materials was considered. The first experiments were done with exfoliated $MoS_2$ and $WSe_2$ deposited on AuNP20. Until now, no evident effect on Raman spectrum or photoluminiscence was observed.

# Bibliography

[1] NOVOSELOV, K. S. et al. Electric field effect in atomically thin carbon films. *Science*, **306**(5696), **2004**, pp. 666–669. DOI: 10.1126/science.1102896.

[2] NOVOSELOV, K. S. et al. Two-dimensional gas of massless Dirac fermions in graphene. *Nature*, **438**(7065), **2005**, pp. 197–200. DOI: 10.1038/nature04233.

[3] XIE, L. et al. Graphene as a substrate to suppress fluorescence in resonance Raman spectroscopy. *Journal of the American Chemical Society*, Citeseer, **131**(29), **2009**, pp. 9890–9891. DOI: 10.1021/ja9037593.

[4] BENEVIDES, J. M., OVERMAN, S. A., THOMAS, G. J. Raman, polarized Raman and ultraviolet resonance Raman spectroscopy of nucleic acids and their complexes. *Journal of Raman Spectroscopy*, Wiley Online Library, **36**(4), **2005**, pp. 279–299. DOI: 10.1002/jrs.1324.

[5] SCHLÜCKER, S. Surface[U+2010]Enhanced raman spectroscopy: Concepts and chemical applications. *Angewandte Chemie International Edition, **53**(19), **2014**, pp. 4756-4795. DOI: 10.1002/anie.201205748.*

[6] CHEN, D. et al. Structure-dependent localized surface plasmon resonance characteristics and surface enhanced Raman scattering performances of quasi-periodic nanoarrays: Measurements and analysis. *Journal of Applied Physics*, **118**(16), **2015**, p. 163101. DOI: 10.1016/S1748-0132(08)70042-2.

[7] VO[U+2010]DINH, T., WANG, H. N. & J. SCAFFIDI. Plasmonic nanoprobes for SERS biosensing and bioimaging. *Journal of biophotonics*, **3**(1,2), **2010**, pp. 89-102. DOI: 10.1002/jbio.200910015.

[8] JARVIS, R. M. & R. GOODACRE. Characterisation and identification of bacteria using SERS. *Chemical Society Reviews*, **37**(5), **2008**, pp. 931-936. DOI: 10.1039/B705973F.

[9] LU, X. et al. Application of mid-infrared and Raman spectroscopy to the study of bacteria. *Food and Bioprocess Technology*, **4**(6), **2011**, pp. 919-935. DOI: 10.1007/s11947-011-0516-8.

[10] LUO, S.-C. et al. Nanofabricated SERS-active substrates for single-molecule to virus detection in vitro: A review. *Biosensors and Bioelectronics*, **61**, **2014**, pp. 232-240. DOI: 10.1016/j.bios.2014.05.013.

[11] STILES, P. L. et al. Surface-Enhanced Raman Spectroscopy. *Annual Review of Analytical Chemistry,* **1**(1), **2008**, pp. 601-626. DOI: 10.1146/annurev.anchem.1.031207.112814.

[12] MILES, R. B., LEMPERT, W. R. & J. N. FORKEY, Laser rayleigh scattering. *Measurement Science and Technology*, **12**(5), **2001**, DOI: 10.1088/0957-0233/12/5/201.

[13] FERRARI A. C. & D. M. BASKO. Raman Spectroscopy as a Versatile Tool for Studying the Properties of Graphene. *Nature Nanotechnology,* **8**(4), **2013**, pp. 235-246. DOI: 10.1038/nnano.2013.46.

[14] DENDISOVÁ, M., ŽVÁTORA, P. & Pavel MATĚJKA. *Ramanova Spektroskopie: Návody k laboratorním úlohám.* [online], [2017-03-25]. Prague University of Chemistry and Technology, Institute of Analytical Chemistry.

[15] SMEKAL, A. Zur quantentheorie der dispersion. *Naturwissenschaften*, **11**(43), **1923**, pp. 873-875. DOI: 10.1007/BF01576902.

[16] SINGH, R. CV Raman and the Discovery of the Raman Effect. *Physics in Perspective,* **4**(4), Springer, **2002**, pp. 399-420. DOI: 10.1007/s000160200002.

[17] INDIAN, J. A new radiation. *Indian Journal Physics*, **2**, **1928**, pp. 387-398. URL:http://repository.ias.ac.in/70648/1/36-PUb.pdf.

[18] RAMAN, C. V. & K. S. KRISHNAN. A new type of secondary radiation. *Nature*, **121**, **1998**, pp. 501–502. DOI: 10.1038/121501c0.

[19] KITAI, Adrian (ed.). *Luminescent materials and applications.* John Wiley Sons, **2008**. ISOBN: 0470985674, 9780470985670.

[20] VANKEIRSBILCK, T. et al. Applications of Raman spectroscopy in pharmaceutical analysis. *TrAC trends in analytical chemistry*, **21**(12), **2002**, pp. 869-877. DOI: 10.1016/S0165-9936(02)01208-6.

[21] HUH, Y. S., CHUNG, A. J. & David ERICKSON. Surface enhanced Raman spectroscopy and its application to molecular and cellular analysis. *Microfluidics and nanofluidics*, **6**(3), Springer, **2009**, p. 285. DOI: 10.1007/s10404-008-0392-3.

[22] DAY, J.S. et al., The detection of drugs of abuse in fingerprints using Raman spectroscopy I: latent fingerprints. *Spectrochimica Acta Part A: Molecular and Biomolecular Spectroscopy*, **60**(3), **2004**, pp. 563-568. DOI: 10.1016/S1386-1425(03)00263-4.

[23] SHEN, H., POLLAK, F. H. & R. N. SACKS, Raman scattering determination of free-carrier concentration and surface space-charge layer in $< 100 >$ n-GaAs. *Applied physics letters*, **47**(8), **1985**, pp. 891-893. DOI: 10.1063/1.95967.

[24] DE WOLF, Ingrid. Micro-Raman spectroscopy to study local mechanical stress in silicon integrated circuits. *Semiconductor Science and Technology*, **11**(2), IOP Publishing, **1996**, p. 139.

[25] WEBER, A. Raman spectroscopy of Gases and Liquids. *Topics in Current Physics*, **11**, Springer Berlin Heidelberg, **2012**. ISBN: 9783642812798.

[26] SCHMID, T. et al. Performing tip-enhanced Raman spectroscopy in liquids. *Journal of Raman Spectroscopy*, **40**(10), **2009**, pp. 1392-1399. DOI: 10.1002/jrs.2387.

[27] MADĚRÁNKOVÁ, D. *Analýza biologicky významných látek.*, Brno University of Technology, Faculty of Electrical Engineering and Communication, **2008**. p. 89. Supervisor Ing. Jiří Roleček.

[28] QIAN, X.-M. & S. M. NIE. Single-molecule and single-nanoparticle SERS: from fundamental mechanisms to biomedical applications. *Chemical Society Reviews*, **37**(5), **2008**, pp. 912-920. DOI: 10.1039/B708839F

[29] ANKER, J. N. et al. Biosensing with plasmonic nanosensors. *Nature materials*, **7**(6), **2008**, pp. 442-453. DOI: 10.1038/nmat2162.

[30] BOKEN, J. et al. Plasmonic nanoparticles and their analytical applications: A review. *Applied Spectroscopy Reviews*, **2017**, DOI: 10.1080/05704928.2017.1312427.

[31] PETRYAYEVA, E. & U. J. KRULL. Localized surface plasmon resonance: nanostructures, bioassays and biosensing—a review. *Analytica chimica acta*, **706**(1), **2011**, pp. 8-24. DOI: 10.1016/j.aca.2011.08.020.

[32] LINIC, S., CHRISTOPHER, P. & D. B. INGRAM. Plasmonic-metal nanostructures for efficient conversion of solar to chemical energy. *Nature materials*, **10**(12), **2011**, pp. 911-921. DOI: 10.1038/nmat3151.

[33] SCHULLER, J. A. et al. Plasmonics for extreme light concentration and manipulation. *Nature materials*, **9**(3), **2010**, pp. 193-204. DOI: 10.1038/nmat2630.

[34] CHEN, Y. & H. MING. Review of surface plasmon resonance and localized surface plasmon resonance sensor. *Photonic Sensors*, **2**(1), **2012**, pp. 37-49. DOI: 10.1007/s13320-011-0051-2.

[35] MAIER, S. A. Plasmonics: fundamentals and applications. *Springer Science Business Media*, **2007**, p. 224. ISBN: 0387378251, 9780387378251.

[36] PALIK, E. D. Handbook of optical constants of solids. *Academic press*, **1998**, p. 804. ISBN: 0080547214, 9780080547213.

[37] ALEX, S., TIWARI, A. Functionalized gold nanoparticles: Synthesis, properties and applications-A review. *Journal of nanoscience and nanotechnology*, **15**(3), 2015, pp. 1869-1894. DOI: 10.1166/jnn.2015.9718.

[38] WEI, H. et al. Polarization dependence of surface-enhanced Raman scattering in gold nanoparticle− nanowire systems. *Nano letters*, textbf8(8), **2008**, pp. 2497-2502. DOI: 10.1021/nl8015297.

[39] LINK, S. & M. A. EL-SAYED. Spectral properties and relaxation dynamics of surface plasmon electronic oscillations in gold and silver nanodots and nanorods. *The Journal of Physical Chemistry B*, **103**(40), **1999**, pp. 8410-8426. DOI: 10.1021/jp9917648.

[40] LINK, S. & M. A. EL-SAYED. Size and temperature dependence of the plasmon absorption of colloidal gold nanoparticles. *The Journal of Physical Chemistry B*, **103**(21), **1999**, pp. 4212-4217. DOI: 10.1021/jp984796o.

[41] KELLY, K. L. et al. The optical properties of metal nanoparticles: the influence of size, shape, and dielectric environment. *The Journal of Physical Chemistry B*, **107**, **2003**, pp. 668-677. DOI: 10.1021/jp026731y.

[42] GOLAB, J. T. et al. A surface enhanced hyper[U+2010]Raman scattering study of pyridine adsorbed onto silver: Experiment and theory. *The Journal of chemical physics*, **88**(12), **1988**, pp. 7942-7951. DOI: 10.1063/1.454251.

[43] XU, W., MAO N. & Jin ZHANG. Graphene: A Platform for Surface-Enhanced Raman Spectroscopy. *Small*, **9**(8), **2013**, pp. 1206-1224. DOI: 10.1002/smll.201203097. ISSN: 16136810.

[44] SCHLUCKER, S., MOSKOVITS M. & H. KNEIPP. *Surface enhanced Raman spectroscopy: analytical, biophysical and life science applications.* Weinheim, Germany: Wiley-VCH Verlag, **22**, **2011**, p. 331. ISBN 978-352-7633-067.

[45] KNEIPP, K., KNEIPP, H. & J. KNEIPP. Surface-enhanced Raman scattering in local optical fields of silver and gold nanoaggregates from single-molecule Raman spectroscopy to ultrasensitive probing in live cells. *Accounts of chemical research*, **39**(7), **2006**, pp. 443-450. DOI: 10.1021/ar050107x.

[46] ZHANG, L. et al. Wrinkled nanoporous gold films with ultrahigh surface-enhanced Raman scattering enhancement. *ACS nano*, **5**(6), **2011**, pp. 4407-4413. DOI: 10.1021/nn201443p.

[47] LIN, Y. Y. et al. Target-size embracing dimension for sensitive detection of viruses with various sizes and influenza virus strains. *Biosensors and Bioelectronics*, **35**(1), **2012**, pp. 447-451. DOI: 10.1016/j.bios.2012.02.041.

[48] LUO, S. C. et al. Nanofabricated SERS-active substrates for single-molecule to virus detection in vitro: A review. *Biosensors and Bioelectronics*, Elsevier, **61**, **2014**, pp. 232-240. DOI: 10.1016/j.bios.2014.05.013.

[49] PALLAORO, A. et al. Rapid identification by surface-enhanced Raman spectroscopy of cancer cells at low concentrations flowing in a microfluidic channel. *Acs Nano*, **9**(4), **2015**, pp. 4328-4336. DOI: 10.1021/acsnano.5b00750.

[50] LI, J. et al. Highly sensitive SERS detection of As3+ ions in aqueous media using glutathione functionalized silver nanoparticles. *ACS applied materials & interfaces*, **3**(10), **2011**, pp. 3936-3941. DOI: 10.1021/am200810x.

[51] LI, N. et al. Identification of Al13 on the Colloid Surface Using Surface-Enhanced Raman Spectroscopy. *Environmental Science & Technology*, **51**(5), **2017**, pp. 2899-2906. DOI: 10.1021/acs.est.6b05721.

[52] FAN, M. et al. A review on the fabrication of substrates for surface enhanced Raman spectroscopy and their applications in analytical chemistry. *Analytica Chimica Acta*, **693**(1), **2011**, pp. 7–25. DOI: 10.1016/j.aca.2011.03.002.

[53] ISHIGAMI, M. et al. Atomic Structure of Graphene on SiO2. *Nano Letters*, **7**(6), **2007**, pp. 1643-1648. DOI: 10.1021/nl070613a. ISSN: 1530-6984.

[54] *Hybridisation of Atomic Orbitals.* [online], [2017-01-29]. Available at: http://butane.chem.uiuc.edu/cyerkes/Chem102AEFa07/Lecture_Notes_102/Lecture%2015%27-102.htm.

[55] *Relativistic wave equations: Graphene.* [online], University of Manchester, **2012**, [2017-04-12]. Available at: http://oer.physics.manchester.ac.uk/AQM2/Notes/Notes-6.4.html.

[56] LEE, C. et al. Measurement of the Elastic Properties and Intrinsic Strength of Monolayer Graphene. *Science*, **321**(5887), **2008**, pp. 385–388. DOI: 10.1126/science.1157996.

[57] YANG, Y. et al. Enhancing graphene reinforcing potential in composites by hydrogen passivation induced dispersion. *Scientific Reports*, **3**(2086), **2013**, pp. 1–7. DOI: 10.1038/srep02086.

[58] CHAWLA, N. & X. DENG. Microstructure and mechanical behavior of porous sintered steels. *Materials Science and Engineering: A*, **390**(1-2), **2005**. pp. 98–112. DOI: 10.1016/j.msea.2004.08.046.

[59] FOGELSTROM, M. Graphene science. *TEDxGoteborg Graphene science*, [online], **2014**, [2017-02-24]. Available at: www.youtube:com=watch?v=eh3dA8xnZ4Y.

[60] PEREIRA, V. M., CASTRO, A. H. & N. M. R. PERES, Tight-binding approach to uniaxial strain in graphene. *Physical Review B*, **80**(4), **2009**, p. 9. PACS numbers: 81.05.Uw,62.20.-x,73.90.+f.

[61] BODENMANN, A. K. & A. H. MACDONALD. Graphene: Exploring carbon flatland. *Physics Today.* **60**(8), **2007**, pp. 35–41. DOI: 10.1063/1.2774096. ISSN: 0031-9228.

[62] CHOI, W. & L. JO-WON. *Graphene: synthesis and applications.* **1**. ROCHA C. G. et al. Boca Raton, CRC Press, **2012**, p. 25. ISBN: 978-1-4398-6187-5.

[63] KOVAŘÍK, Š. *Selektivní hydrogenace grafenu připraveného metodou chemické depozice z plynné fáze.* Brno University of Technology, Faculty of Mechanical Engineering, **2016**. p. 28. Supervisor Ing. Miroslav Bartošík, Ph.D.

[64] BAEUMER, C. et al. Ferroelectrically driven spatial carrier density modulation in graphene. *Nature communications*, Nature Publishing Group, **6**(6136), **2015**, p. 8. DOI: 10.1038/ncomms7136.

[65] CASIRAGHI C. et al. Raman Fingerprints of Charged Impurities in Graphene. *Applied Physics Letters*, AIP, **91**(23), **2007**. DOI: 10.1063/1.2818692.

[66] SCHWIERZ, F. Graphene transistors. *Nature Nanotechnology*, **5**, **2010**. pp. 487–496. DOI: 10.1038/nnano.2010.89.

[67] Raccichini, R. et al. The role of graphene for electrochemical energy storage. *Nature Materials*, **14**(3), **2015**, pp. 271–279. DOI: 10.1038/nmat4170.

[68] KNEIPP, K. et al. *Surface-enhanced raman scattering: physics and applications.* New York: Springer, **17**, **2006**, p. 464. ISBN 978-354-0335-665.

[69] LING, X. et al., Can Graphene be used as a Substrate for Raman Enhancement? *Nano Letters.* **10**(2), **2010**, pp. 553-561. DOI: 10.1021/nl903414x. ISSN: 1530-6984.

[70] LING, X. et al. Probing the Effect of Molecular Orientation on the Intensity of Chemical Enhancement Using Graphene[U+2010]Enhanced Raman Spectroscopy. *Small*, **8**(9), **2012**, pp. 1365-1372. DOI: 10.1002/smll.201102223.

[71] MARTYSHKIN, D. V. et al. Effective suppression of fluorescence light in Raman measurements using ultrafast time gated charge coupled device camera. *Review of Scientific Instruments*, AIP, **75**(3), **2004**, pp. 630-635.

[72] LIU, Y., HU, Y. & J. ZHANG. Few-layer graphene-encapsulated metal nanoparticles for surface-enhanced Raman spectroscopy. *The Journal of Physical Chemistry C*, ACS, **118**(17), **2014**, pp. 8993-8998. DOI: 10.1021/jp500751a.

[73] Kolíbal, M. et al. Guided Assembly of Gold Colloidal Nanoparticles on Silicon Substrates Prepatterned by Charged Particle Beams. *ACS Nano*, **6**(11), **2012**, pp. 10098–10106. DOI: 10.1021/nn3038226.

[74] LIGMAJER, F. *Uspořádaná a neuspořádaná pole koloidních nanočástic a jejich využití pro detekci biomolekul.* Brno University of Technology. Faculty of Mechanical Engineering, **2013**. p. 62. Supervisor Ing. Miroslav Kolíbal, Ph.D.

[75] PROCHÁZKA, P. *Příprava grafenu metodou CVD.* Brno University of Technology. Faculty of Mechanical Engineering, **2012**. p. 65. Supervisor Ing. Jindřich Mach, Ph.D.

# List of abbreviations

| | |
|---|---|
| 2D | Two-dimensional |
| SERS | Surface-enhanced Raman spectroscopy |
| SPP | Surface plasmon polariton |
| LSP | Localized surface plasmon |
| GSH | Glutathione |
| 4-MPY | 4-mercaptopyridine |
| GERS | Graphene-enhanced Raman scattering |
| UV-RRS | Ultraviolet resonance Raman spectroscopy |
| DNA | Deoxyribonucleic acid |
| RNA | Ribonucleic acid |
| AuNPs | Gold colloidal nanoparticles of size s |
| HF | Hydrogen fluoride |
| SP | Surface potential |
| KPFM | Kelvin Probe Force Microscopy |
| AFM | Atomic Force Microscopy |
| CVD | Chemical vapor deposition |
| PMMA | Poly-methyl methacrylate |
| R6G | Rhodamine 6G |